Prokocki Eric (Orcid ID: 0000-0002-4942-9858)

Ashworth Philip (Orcid ID: 0000-0002-9642-4857)

The morphology of fluvial-tidal dunes: Lower Columbia River, OR/WA, USA

Prokocki, E.W.[1,2], Best, J.L.[2,3], Perillo, M.M.[4], Ashworth, P.J.[5], Parsons, D.R.[6], Sambrook Smith, G.H.[7], Nicholas, A.P.[8], Simpson, C.J.[9]

[1]Department of Geosciences, Florida Atlantic University, 777 Glades Road, Boca Raton, FL 33431, USA (Email: ewaschle2@gmail.edu)
[2]Department of Geology, University of Illinois, 1301 West Green Street, Urbana, IL 61801, USA
[3]Departments of Geography & GIS and Mechanical Science and Engineering, and Ven Te Chow Hydrosystems Laboratory, University of Illinois, 1301 West Green Street, Urbana, IL 61801, USA (Email: jimbest@illinois.edu)
[4]ExxonMobil Exploration Company, 22777 Springwoods Village Parkway, Spring, TX 77389, USA (Email: mauricio.m.perillo@exxonmobil.com)
[5]School of Applied Sciences, University of Brighton, Brighton, Sussex BN2 4GJ, UK (Email: p.ashworth@brighton.ac.uk)
[6]Department of Geography, Environment and Earth Sciences, Faculty of Science and Engineering, University of Hull, Hull, HU6 7RX, UK
(Email: d.parsons@hull.ac.uk)
[7]School of Geography, Earth, Environmental Sciences, University of Birmingham, Edgbaston, Birmingham, B15 2TT, UK
(Email: g.smith.4@bham.ac.uk)
[8]Department of Geography, College of Life and Environmental Sciences, University of Exeter, EX4 4RJ, UK
(Email: a.p.nicholas@exeter.ac.uk)
[9]Fulcrum Graphic Communications Inc., Airdrie, Alberta, Canada
(Email: chris_simpson@outlook.com)

Corresponding Author

Eric W. Prokocki, Department of Geosciences, Florida Atlantic University, 777 Glades Road, Boca Raton, FL, 33431, USA, (Email: ewaschle2@gmail.com)

ACKNOWLEDGEMENTS

This research was funded primarily by ExxonMobil, but was also supported by UK Natural Environment Research Council (NERC) grant awards NE/H007954/1, NE/H006524/1, NE/H007261/1 and NE/H00582X/1. We thank Mike Blum and Howard Feldman for their encouragement during this research, and the Clatsop Community College and Environmental Research and Training Station for providing additional resources and support. We graciously thank Michael Wilkin, Katie Rathmell and António Baptista, for their advice and expertise regarding the lower

Columbia River, as well as Hans Moritz from the Portland District office of the US Army Corp of Engineers (USACE) for providing information regarding the timing, boundaries, and effects, of federal navigation channel dredging operations from 2005-2010. We also thank Pat Killion, captain of the Tansey Point, whose years of experience on the lower Columbia River were paramount towards enabling this research. Lastly, we especially thank Bob Dalrymple for his extremely insightful and stimulating review, as well as the thorough reviews from one anonymous referee and editor that greatly improved the paper.

AUTHOR CONTRIBUTIONS

E.W. Prokocki: conceptualisation (co-lead); investigation (lead); writing – original draft (lead); formal analysis (lead); writing – review and editing (lead); investigation (lead); methodology (co-lead); software (co-lead); project administration (co-lead); visualisation (co-lead). **J.L. Best**: conceptualisation (co-lead); funding acquisition (co-lead); project administration (co-lead); resources (co-lead); writing – original draft (supporting; equal); writing – review and editing (supporting; equal). **M.M. Perillo**: conceptualisation (co-lead); investigation (supporting); formal analysis (supporting); methodology (co-lead); software (co-lead); writing – original draft (supporting). **P.J. Ashworth**: funding acquisition (co-lead); project administration (co-lead); resources (co-lead); writing – original draft (supporting; equal); writing – review and editing (supporting; equal). **D.R. Parsons**: writing – original draft (supporting). **G.H. Sambrook Smith**: writing – original draft (supporting; equal); writing – review and editing (supporting; equal). **A.P. Nicholas**: writing – original draft (supporting). **C.J. Simpson**: software (supporting); visualisation (supporting; equal).

DATA AVAILABILITY STATEMENT

The bathymetric data of the Lower Columbia River was collected by the National Oceanographic and Atmospheric Administration (NOAA) and is available for open-access download at https://www.ncei.noaa.gov/maps/bathymetry/ using the bathymetric data viewer. Data plotted and visualised in this article is available through the corresponding author upon request.

ABSTRACT

This paper quantifies changes in primary dune morphology of the mesotidal Lower Columbia River (LCR), USA, through ~ 90 river kilometres of its fluvial-tidal transition at low-river stage. Measurements were derived from a Multibeam Echo Sounder dataset that captured bedform dimensions within the thalweg (≥ 9m depth; H/H_{max} ≥ 0.7) of the LCR main channel. Measurements revealed two categories of dunes: i) fine to medium sand 'fluvial-tidal to tidal' (upstream-oriented, simple, and 2D) low-

angle dunes (heights ≈ 0.3-0.8m; wavelengths ≈ 10-25m; mean lee-angles ≈ 7-11°), and ii) medium to coarse sand 'fluvial' (downstream-oriented, compound, and 2.5-3D) low-angle dunes (heights ≈ 1.5-3m; wavelengths ≈ 60-110m; mean lee-angles ≈ 11-18°). At low-river stage, where H/H_{max} ≥ 0.7, approximately 86% of the fluvial-tidal transition is populated by 'fluvial' dunes, whilst ~ 14% possesses 'fluvial-tidal to tidal' dunes that form in the downstream-most reaches. Thus, throughout the majority of the deepest channel segments of the fluvial-tidal transition, seaward-oriented river and ebb-tidal currents govern dune morphology, whilst strong bidirectional tidal-current influence is restricted to the downstream most reaches of the transition zone. Two mechanisms are reasoned to explain dune low-angle character: (1) high-suspended sediment transport near peak tidal-currents that lowers the leeside-angles of 'fluvial-tidal to tidal' dunes, and (2) superimposed bedforms that erode the crests, leesides, and stoss-sides, of 'fluvial' dunes, which results in the reduction of leeside-angles. Fluctuations in river discharge create a 'dynamic morphology reach' at depths where H/H_{max} ≥ 0.7, which spans river kilometres 12-40 and displays the greatest variation in dune morphology. Similar channel reaches likely exist in fluvial-tidal transitions with analogous physical characteristics as the Lower Columbia River and may provide a distinct signature for the fluvial-tidal transition zone.

Keywords: Lower Columbia River, fluvial-tidal bedforms, low-angle dunes, superimposed bedforms, tidal bedforms

1 INTRODUCTION

Bedforms are ubiquitous within subaqueous environments and are generated by unidirectional, short to long period oscillatory, and combined-flows (currents with unidirectional and oscillatory components), which deform a mobile bed through

erosion and deposition of sediment. For centuries, laboratory, field and theoretical investigations have focused on bedform genesis, morphological equilibrium, and their depositional structures (e.g., Du Buat, 1786; Blasius, 1910; Kennedy, 1969; Harms et al., 1975; Allen, 1983; Southard, 1991; Baas, 1994; Kleinhans, 2001; Venditti et al., 2005a,b; Doucette and O'Donoghue, 2006; Reesink and Bridge, 2009; Perillo et al., 2014a,b,c; Bradley and Venditti, 2019a,b). One of the most common subaqueous bedforms are dunes (Best, 2005; Venditti, 2013), whose strata represent a fundamental building block of the rock record (Ashley, 1990; Myrow and Southard, 1991; Myrow et al., 2002; Bridge, 2003; Martinius and Van den Berg, 2011; Reynaud and Dalrymple, 2012). Subaqueous dunes typically possess heights of 0.075 to > 5m, wavelengths from 0.6 to > 100m, and can be compound (possessing crests, stoss-sides, or leesides, populated with smaller-scale superimposed bedforms) or simple (lacking superimposed bedforms) in form (Dalrymple et al., 1978; Dalrymple, 1984; Ashley, 1990). Primary (largest) and secondary (superimposed) dune morphology is a function of the interplay between growth, migration, and decay, as controlled by varying current magnitudes and orientations (cf. Dalrymple et al., 1978; Sherwood and Creager, 1990; Dalrymple and Rhodes, 1995; Hendershot et al., 2016) in conjunction with changes in the ratio of bedload, q_{bed}, to suspended-load, q_{sus}, transport rates (q_{sus}/q_{bed}; Amsler and Schreider, 1999; Best, 2005; Hendershot et al., 2016; Bradley and Venditti, 2017; Ma et al., 2017; Naqshband and Hoitink, 2020). Dunes are therefore spatially and temporally dynamic and follow coupled flow and sediment transport hysteresis loops (Allen, 1974, 1976; Martin and Jerolmack, 2013; Parsons and Best, 2013), which result in transient morphologic properties (Dalrymple et al., 1978; Bradley and Venditti, 2019a,b). These properties include height (η), wavelength (λ), aspect ratio

(AR), lee- and stoss- side angles (θ_{lee} and θ_{stoss}, respectively), dimensionality (2 to 3D), roundness, symmetry, and scaling of η and λ to a characteristic flow depth, H, which typically is taken as local (mean) depth, H_{mean}, or maximum depth, H_{max}. Thus, capturing how changes in dune morphology induce variations in flow-fields via form drag (Smith and McLean, 1977; Parsons et al., 2005; Sukhodolov et al., 2006; Guerrero and Lamberti, 2011; Lefebvre et al., 2011), which affects their migration rates and thus bedload transport rates (cf. Nittrouer et al., 2008; Gómez et al., 2010; Knox and Latrubesse, 2016; Schippa et al., 2016), is vital towards building more robust hydraulic and morphodynamic models (cf. Sandbach et al., 2018; van de Lageweg and Feldman, 2018; van de Lageweg et al., 2018; Unsworth et al., 2020).

Based upon longitudinal profiles (e.g., θ_{lee}, symmetry, and roundness), past work has divided subaqueous dunes into two categories (Kostaschuk and Villard, 1996, 1999; Venditti, 2013): high-angle dunes (HADs) and low-angle dunes (LADs). High-angle dunes tend to be asymmetric and often are only slightly rounded, with long, gentle θ_{stoss} and short, steep θ_{lee} near, or at, the angle-of-repose (~ 25-30°). They have been speculated to be observed commonly in bedload dominated laboratory flumes and shallow (H < 2.5m) rivers (cf. Venditti and Bauer, 2005; Bradley and Venditti, 2017), but have also been observed in the tidally-dominated, Cobequid Bay, Canada (Dalrymple, 1984). In contrast, low-angle dunes possess mean θ_{lee} below the angle-of-repose (typically ≤ 15° in deep rivers where H ≥ 2.5m, Best and Kostaschuk, 2002; Best, 2005; Kostaschuk et al., 2009; Bradley and Venditti, 2017; Cisneros et al., 2020; and ≤ 10° in estuarine settings, Dalrymple and Rhodes, 1995), and especially in rivers can be more rounded and symmetric. Furthermore, experimental (Best and Kostaschuk, 2002), numerical (Lefebvre, 2019; Lefebvre and Winter, 2016; Lefebvre et al., 2014a,b), and field studies (Smith and

McLean, 1977; Kostaschuk and Villard, 1996; Williams et al., 2003; Holmes and Garcia, 2008; Kostaschuk et al., 2009; Bradley et al., 2013; Cisneros et al., 2020), suggest that flow separation over LAD leesides is intermittent (θ_{lee} ~ 10-24°) to non-existent (θ_{lee} < 10°), whilst HADs possess continuous leeside flow separation.

Three modern environments have received the most attention regarding dune morphology: i) relatively deep (H ≥ 2.5 m; Bradley and Venditti, 2017) rivers (e.g., Harbor, 1998; Nittrouer et al., 2008, 2011; Sambrook Smith et al., 2013; de Almeida et al., 2016; Knox and Latrubesse, 2016; Bradley and Venditti, 2017; Galeazzi et al., 2018; Kostaschuk and Venditti, 2019; Cisneros et al., 2020), ii) shallow marine combined flow wave-tidal settings (Carle and Hill, 2009; Ernstsen et al., 2010; Barnard et al., 2011; Lefebvre et al., 2011; Fraccascia et al., 2016; Wu et al., 2016), and iii) meso- to macro- tidal estuaries or deltas (e.g., Langhorne, 1973; Wright et al., 1973; Dalrymple et al., 1978; Elliot and Gardiner, 1981; Dalrymple, 1984; Aliotta and Perillo, 1987; Harris, 1988; Davis and Flemming, 1991; Sherwood and Creager, 1990; Dalrymple and Rhodes, 1995; Gómez et al., 2010; Hendershot et al., 2016). Two advances in quantifying dune morphology are measurements of θ_{lee} that focus on the prevalence and physical causes of LADs *vs* HADs (e.g., Dalrymple and Rhodes, 1995; Hendershot et al., 2016; Kostaschuk and Venditti, 2019; Cisneros et al., 2020), and the re-evaluation of existing η and λ to H scaling relations (Bradley and Venditti, 2017, 2019a; Cisneros et al., 2020). Ever since the proposition of empirical scaling relations ($\eta = 0.17H$; $\lambda = 5H$) by Yalin (1964) and Allen (1982), it has been widely adopted (although not universally accepted; see Dalrymple and Rhodes, 1995; Bradley and Venditti, 2017) that dune η and λ scale to boundary layer thickness (Allen, 1968; Ashley, 1990; Southard and Boguchwal, 1990a,b; Best, 2005), which can be no greater than H_{max}. In more recent work, Bradley and Venditti

(2017) examined how formative hydraulics and sediment transport processes change as dunes grow with increasing H and modified the original relations to $\eta = 0.13H$ and $\lambda = 5.9H$, whereas dune analyses from multiple rivers (Cisneros et al., 2020) found that the relation for η should be closer to $\eta = 0.10H$. However, regardless of the scaling relation, field data from modern river and tidal settings place the normalised dune η (η/H) and λ (λ/H) within the ranges of ~ 0.025-0.4 and 1-16, respectively (Allen, 1982; Dalrymple and Rhodes, 1995; Venditti, 2013; Bradley and Venditti, 2017; Cisneros et al., 2020).

As the number of mean θ_{lee} (average of leeside angles measured from crest to the bottom of the downstream trough) and maximum θ_{lee} (slipface angle) measurements of dunes from modern environments increases, it is apparent that silt- to gravel- bed rivers, estuaries, and deltas can be dominated by simple and compound low-angle dunes (e.g., Dalrymple and Rhodes, 1995; Hendershot et al., 2016; Bradley and Venditti, 2017; Ma et al., 2017; Kostaschuk and Venditti, 2019; Cisneros et al., 2020). The physical processes driving their formation, however, remain debated (Best and Fielding, 2019; Best et al., 2020), with proposed mechanisms for compound low-angle dunes being: i) erosion of primary dune crests and leesides via heightened localised bed shear stresses generated by superimposed bedforms (Allen and Collinson, 1974; Allen, 1978; Reesink and Bridge, 2009), and/or restriction of bedload supply to the primary dune crest by superimposed bedforms, which starves them of sediment needed to maintain steep slipfaces with sediment avalanches (Carling et al., 2000; Sukhodolov et al., 2006); ii) superimposed bedforms may suppress flow separation over the crests of primary dunes (Dalrymple and Rhodes, 1995; Best et al., 2020); and iii) development of compound dunes at oblique orientations relative to the local flow direction can

suppress flow separation due to the apparent leeside angle being smaller than the true leeside angle (Allen, 1968; Sweet and Kocurek, 1990; Dalrymple and Rhodes, 1995). Alternatively, the proposed mechanisms for simple low-angle dunes include: i) the shift of sediment deposition, from dune crests to dune leesides and/or lee-troughs, caused by higher rates of suspended-sediment transport, which reduces the sediment available to maintain a steep slip-face with avalanches (Smith and McLean, 1977; Bridge and Best, 1988; Kostaschuk and Villard, 1996; Kostaschuk et al., 2009; Hendershot et al., 2016; Bradley and Venditti, 2017; Ma et al., 2017; Naqshband and Hoitink, 2020); ii) downslope lee-face currents resulting from intermittent to non-existent flow separation over the dune leeside (Kostaschuk and Venditti, 2019), and iii) liquefied grainflows produced by high excess pore pressures that cause failure of dune brinkpoint wedge deposits (Hendershot et al., 2016; Kostaschuk and Venditti, 2019), although this mechanism seems unlikely based on abundant morphological data (Best et al., 2020). There is insufficient evidence to suggest that any one mechanism (for either simple or compound low-angle dunes) explains unequivocally their prevalence (see Kostaschuk and Venditti, 2019; Cisneros et al., 2020), or that the mechanisms proposed for simple dunes do not also play some role in the formation of compound dunes. For example, in sand-bed (200-900μm) rivers, simple and compound low-angle dunes coincide with estimated q_{sus}/q_{bed} ratios of > 2.3 (Kostaschuk and Venditti, 2019), whilst in the low Froude number (0.17 < Fr < 0.30) experiments of Naqshband and Hoitink (2020) designed to mimic deep rivers, lee-angles of simple dunes progressively lowered via the onset of increasingly higher rates of suspended-sediment transport. Overall, this evidence suggests that the q_{sus}/q_{bed} ratio likely plays some role in both simple and compound low-angle dune formation.

Four principal deficiencies persist in our understanding of the morphology of fluvio-tidal dunes. First, although studies tend to report η, λ, aspect ratios, and θ_{lee}, they rarely quantify dimensionality, roundness, and symmetry, via standardised parameters (cf. Harms, 1969; Arnott and Southard, 1990; Oost and Baas, 1994; Dumas et al., 2005; Venditti et al., 2005a,b; Sekiguchi and Yokokawa, 2008; Perillo et al., 2014a,b,c), although notable exceptions include the studies by Dalrymple et al. (1978), Dalrymple (1984), Dalrymple and Rhodes (1995), and Hendershot et al. (2016). Secondly, many studies of river deltas are spatially restricted to either unsteady and non-uniform 'backwater' channel reaches, or to steady and uniform 'normal flow' reaches (but see Harbor, 1998, for an exception). Thus, few studies capture the broader pattern changes driven by upstream to downstream variations in channel bed grain size in conjunction with changes in mean flow hydraulics (see Mei et al., 2021). Additionally, many studies only report findings acquired over short temporal windows that are fixed to a narrow range of river stages, which makes it impossible to evaluate sediment transport regime and hysteresis effects caused by discharge variations (cf. Bradley and Venditti, 2019a, b; Naqshband and Hoitink, 2020). Thirdly, estuarine studies tend to be spatially confined to the lowermost backwater reaches, which possess relatively low fluvial input and are thus dominated by bidirectional currents (Dalrymple and Rhodes, 1995; Gómez et al., 2010). Furthermore, few studies have investigated temporal fluctuations over tidal-cycles (see Dalrymple et al., 1978; Sherwood and Creager, 1990; Hendershot et al., 2016), or captured upstream to downstream variations in bedform morphology (Sherwood and Creager, 1990) that are linked to changes in grain size and spatio-temporal changes in tidal- and fluvial- flow.

To address several of these limitations, the present study analyses the primary dunes within the deepest (≥ 9m depth from Mean Sea-Level, MSL, or local H/H_{max} ≥ 0.7) portions of the main channel of the mesotidal Lower Columbia River (LCR), OR/WA, USA, using a multibeam echo sounder (MBES) dataset collected by the National Oceanic and Atmospheric Administration (NOAA) through ~ 90 river kilometres (rkm) of its fluvial-tidal transition (FTT; Dalrymple and Choi, 2007, or fluvial-tidal zone; Van den Berg et al., 2007; Figure 1). Since FTTs are sensitive to sea-level rise and are host to a large proportion of the world's population, spatial characterisation of primary dune morphology can inform hydraulic and morphodynamic models used for assessing flood risk, ecological sustainability, and remediation/dredging strategies. Three questions are addressed herein:

1) How does primary dune morphology vary through the LCR fluvial-tidal transition?

2) Do variations in dune morphology relate to transitions in hydraulic and sediment transport processes, and/or bed grain size?, and

3) How does dune morphology differ from tidally-dominated estuaries and unidirectional current-dominated rivers and flume experiments?

2 STUDY SITE: LOWER COLUMBIA RIVER

The mean annual discharge, Q_{Wavg}, of the Lower Columbia River is ~ 7,000 m^3s^{-1} at the Port Westward (Beaver) gauge station (~ rkm 85) near the upstream margin of the study reach (Figures 1 and 2A; Naik and Jay, 2011). Low and high- river stages are herein classified as those less or greater than 7,000 m^3s^{-1}, respectively. Peak

contemporary flows, Q_{Wpeak}, are constrained by dam releases to between ~ 15,000-17,000m^{3}s^{-1} (Gelfenbaum, 1983; Naik and Jay, 2011; Simenstad et al., 2011), which are lower than pre-1900s 'natural' spring freshets (≥ 18,000m^{3}s^{-1}; Naik and Jay, 2011; Figure 2A). The LCR channel bed slope, S_c, is ~ 1.15 x 10^{-5} (Hickson, 1912; Figure 2A), and is influenced by mixed diurnal and semidiurnal tides within a mesotidal regime. At its mouth, the mean diurnal tidal prism, Q_{tide}, is ~ 11.0 x 10^8 m^3 (Walton and Adams, 1976) and the mean tidal range and highest astronomical tide are 1.7 and 3.6m, respectively, which rise marginally to 2.0 and 4.0m near Astoria, as the result of tidal funnelling (Figure 2A; Fain et al., 2001; Simenstad et al., 2011). The LCR hydrographic ratio, H_g, defined as $\left(Q_{tide}/Q_{Wavg}\right)\ x\ 6hrs$, is equal to 7 (where H_g < 10 reflects fluvial dominance; Peterson et al., 1984), where this fluvial dominance is also supported by the results from hydrodynamic modelling (Hamilton, 1990; Sandbach et al., 2018). Yet, in contrast to this finding, many oceanographic and geologic studies describe the Lower Columbia River as an estuary (e.g., Hughes and Rattray, 1980; Gelfenbaum, 1983; Fox et al., 1984; Jay, 1984; Hamilton, 1990; Jay and Smith, 1990; Jay et al., 1990; Sherwood and Creager, 1990; Simenstad et al., 2011; Peterson et al., 2013, 2014). However, its geologic designation as an estuary has been re-evaluated by Prokocki et al. (2015, 2020), who suggest that the mid to late Holocene geomorphology of the LCR is that of an 'entrenched' fluvio-deltaic environment possessing a subaqueous deltaic top-set extending to ~ rkm 50, thus supporting fluvial dominance, whilst providing a physical explanation for its geomorphic designation as an estuary.

With respect to the LCR fluvial-tidal transition, Jay et al. (1990) computed the temporally-averaged mean flux divergence of fluvial vs tidal potential-energy through modern channel-sections, and used this to divide the LCR into three hydraulic zones

(Figs 2B and 3A): 1) The tidally-dominated regime (TDR; rkm 0-21), or lower delta, which experiences bidirectional tidal-currents, saltwater intrusion, and development of a turbidity maximum (TM; Fox et al., 1984; Sherwood and Creager, 1990); 2) The mixed tidal-fluvial regime (MTFR; ~ rkm 21-56; or upper brackish water delta to lower freshwater tidal river reach; Hoitink and Jay, 2016), where fluvial- and bidirectional tidal- currents compete for dominance; and 3) The fluvially-dominated, tidally-influenced regime (FDTIR; ~ rkm 56-235; or mid to upper freshwater tidal river reach; Hoitink and Jay, 2016), which is governed by downstream-oriented currents and terminates at the landward most point of tidally-forced variations in water surface elevation, or the tidal limit. However, like all FTTs (Dalrymple and Choi, 2007; Dalrymple et al., 2015), the longitudinal boundaries of these LCR regimes expand or contract in accordance with spring to neap tidal-cycles and varying river-stages. For example, during the transition from high- to low- river stage, the upstream boundaries of the TDR, MTFR, and FDTIR, expand to ~ rkm 35, 109, and 235 (Bonneville Dam; i.e., tidal limit), respectively, which causes (Figure 3A): i) brackish water intrusion to ~ rkm 50 (Fox et al., 1984; Chawla et al., 2008), ii) fluvial current reversals between rkm 50 to ~ 109 (Clark and Snyder, 1969), and iii) tidally-induced cyclic water surface height variations beyond rkm 172 (Vancouver, WA; Kukulka and Jay, 2003). Thus, during low-river stages, ~ rkm 0 to 35 (zones 1-5; hereafter z1-z5) is mainly dominated by tidal flows (Figure 3B), whilst ~ rkm 35-90 (zones 6-11; hereafter z6-z11) experiences a downstream to upstream increase in fluvial-energy as tidal influence diminishes (Figure 3B).

The mean annual sediment-load, Q_s, of the Lower Columbia River where $Q_s = Q_{sand} + Q_{wash}$ (Q_{sand} represents bedload + suspended-load particles (> 63 to ≤ 2000μm), and Q_{wash} represents suspended-load particles ≤ 62 μm), is sourced from

tributaries upstream of ~ rkm 172 (Jay et al., 1990; Sherwood et al., 1990; Naik and Jay, 2011), whilst negligible Q_s is derived from continental shelf sources (Gelfenbaum et al., 1999; Templeton and Jay, 2013). Prior to the 1900s, Q_s in the LCR is estimated to have been ~ 10 Mtyr^{-1} (Sherwood et al., 1990; Gelefenbaum et al., 1999; Naik and Jay, 2011), but more recent estimates suggest that after 1970 (post-dam era) Q_s has decreased by ~ 70% to ~ 3.2 Mtyr^{-1} (Naik and Jay, 2011). Grain size sampling of deep (H/H_{max} ≥ 0.7) channel-beds (Fox et al., 1984; Sherwood and Creager, 1990), shows that its D_{50} is fine sand (> 125 to 250μm) from ~ rkm 0 to 32, but increases to medium to coarse sands (> 250 to < 1000μm) upstream of rkm 32 (Figure 3B). This breakpoint in D_{50} tends to remain spatially fixed during both low- and high- river stages, but during significant river floods, minimal coarsening of the channel-bed from fine to fine-medium sand (> 125 to ~ 275μm) may occur between ~ rkm 16-32 (Sherwood and Creager, 1990).

Previous analyses of primary dunes (≥ 9m depth; H/H_{max} ≥ 0.7) in seaward channel reaches of its fluvial-tidal transition (Sherwood and Creager, 1990) recognized three types (see summary of morphology in Table 1). The Type-A dunes occurred between ~ rkm 0-9, were simple in form, developed under significant suspended-sediment transport conditions, and remained tidally-reversing during both low- and high- river stages (Figure 4A, B). Conversely, Type-B were also simple in form and existed between ~ rkm 9-35 during low-river stages, but were restricted to between ~ rkm 9-16 during high-river stages (Figure 4A, B). These dunes also formed within high suspended-sediment transport conditions, and during high-river stages possessed lee-faces that remained downstream oriented over tidal-cycles, but during low-river stages, they maintained upstream orientations (Figure 4A, B). The Type-C compound dunes were the coarsest grained and were confined to

upstream of ~ rkm 30 during low-river flow, but extended downstream to ~ rkm 24 at high-river stage (Figure 4A, B). Throughout all tidal-cycles and river-stages, Type-C dunes remained downstream-oriented and formed within lower suspended-sediment transport conditions relative to Type-A and B. These descriptions and categorisation (Table 1), however, are limited in four ways: i) the number (N) of dunes analysed was not provided, and observations were restricted to ~ rkm 0-35, ii) η, ʎ, and aspect ratios, were reported as general ranges without mean values, and mix both low- and high- river stage observations, iii) dune symmetry, roundness, and dimensionality were not quantified using a standard set of methods, and iv) fundamental properties, such as leeside-angles and scaling of η and ʎ to flow depth, were not measured.

3 METHODS OF ANALYSIS

The low-river stage (< 7,000 m^3s^{-1}; Table 2) bathymetry dataset utilised (~ rkm 0-90, z1-z11; Figures 1 and 3B) herein represents an integration of NOAA bathymetry soundings from multiple survey systems, whose horizontal and vertical positions were acquired using the Differential Global Positioning System (DGPS). Thus, the integrated 3D surface maps analysed possess horizontal and vertical resolutions of ~ 0.5 to 0.05m and ~ 0.05m, respectively. Soundings at sites z1-8 (Figure 1) are normalised to the Mean Lower-Low Water (MLLW) level at the NOAA Astoria tide gauge (ID: 9439040), whilst z9-11 soundings are normalised to the Columbia River Datum, which approximates the extension of the MLLW at Astoria, OR, above ~ rkm 48 (Stolz et al., 2005). Surveys either occurred (Table 2): i) simultaneously with 2005-2010 dredging of the navigation channel (z1-7, and z9-11), or ii) immediately after 2010 dredging (~ rkm 40-48; z8). Therefore, recently dredged channel segments outside or within the zones analysed were identified and excluded from

analysis (see Supporting Information: Type 1 and 2 dredged channel beds) to evaluate only unmodified bedforms (Figures 5-8). Next, in each zone, 2D bed transects were sampled at 1cm horizontal spacing perpendicular to bedform crestlines. The location of these transects are shown in Figures 5-8, whilst example partial sectional-profiles (A-A' to K-K' in Figures 5-8) are displayed in Figure 9. Note that the horizontal spacing of points (1cm) within transects are ≤ the horizontal and vertical resolutions of 3D surface maps in order to ensure the most detailed analysis of bedform geometries, and all bedforms evaluated occur at depths ≥ 9m (localised H/H_{max} ≥ 0.7; Figures 5-8) to remain consistent with previous Lower Columbia River bedform analyses.

Following Hendershot et al. (2016), individual bed features from all zones were detected automatically within 2D transects using a Matlab script (Perillo et al., 2014a) that identifies consecutive local minimum-maximum-minimum bed elevation points along sectional-profiles (Figure 10A). The η values of all identified bed features were then computed. At this stage, the computed η values of bed features includes both primary and secondary (superimposed) bedforms (Figure 10A). However, to compare and integrate the present findings with that of the primary dunes examined by Sherwood and Creager (1990), all secondary bedforms were filtered from the zone data. Therefore, a cut-off value for a primary dune η was established by finding the maximum secondary bedform η within zone transects via hand measurements. For each zone, these values thus represent the breakpoint in η between primary dunes and secondary bedforms (Figure 10B and Table 3), where the primary dunes of a given zone must possess η > the maximum η of secondary bedforms. However, since the η of primary dunes, and thus also the maximum η of secondary bedforms, differs between zones (Figures 9 and 10A), a unique primary

dune η cut-off value was utilised for each zone (Table 3). After applying the primary dune η cut-offs, the wavelengths, ʎ, of remaining primary dunes were calculated as the distance between upstream and downstream minimum trough elevations (Figure 10B). The primary dunes of each zone were then further characterised by quantifying the following geometric properties.

Dune aspect ratio was calculated as:

$$\mathrm{AR} = \lambda/\eta \qquad (1)$$

whereas dimensionality (crestline sinuosity) was measured following the approach of Venditti et al. (2005a), who defined a non-dimensional span index, NDS, as:

$$\mathrm{NDS} = \mathrm{L_c}/\mathrm{L_y} \qquad (2)$$

where $\mathrm{L_c}$ represents the measured length of a dune crestline, and $\mathrm{L_y}$ is the straight-line distance between the ends of this same crestline (Figure 11A). The following values were used to classify bedform sinuosity:

- NDS < 1.08 = 2D
- NDS ≥ 1.08 < 1.16 = 2.5D
- NDS ≥ 1.16 = 3D

Bedform symmetry and roundness indices (BSI and BRI, respectively) were computed (Tanner, 1967; Perillo et al., 2014a) using:

$$\mathrm{BSI} = \lambda_{\mathrm{stoss}}\lambda_{\mathrm{lee}}^{-1} \qquad (3)$$

$$\mathrm{BRI} = \lambda_{0.5_{\mathrm{stoss}}}\lambda_{\mathrm{stoss}}^{-1} \qquad (4)$$

where λ_{stoss} is stoss-side length, λ_{lee} is leeside length, and $\lambda_{0.5_{\mathrm{stoss}}}$ represents the length from dune crest to stoss-side at 0.5η (Figure 11B), where the sectional form boundaries were classified as (Perillo et al., 2014a):

- BSI > 1.5 = Asymmetric
- BSI ~ 1.3-1.5 = Quasi-asymmetric
- BSI < 1.5 = Symmetric
- BRI ≥ 0.6 = Rounded
- BRI < 0.6 = Not rounded

Next, maximum and mean θ_{lee} values were determined utilising the procedures and relations given in Figure 11C. Individual measurements were conducted by visualizing singular dune profiles within the Global Mapper software, and then calculating all leeside angles via the slope measurement tool. Recent research (Lefebvre and Winter, 2016; Cisneros et al., 2020) has illustrated the complexity of dune leeside shape, which is often segmented with lower angle slopes both near the crest and trough of the dune. To account for this complexity, the maximum, as well as the mean, leeside angles were quantified (see definitions in Figure 11c). Lastly, scaling of mean η and λ to mean flow depth, H_{mean}, was assessed, where H_{mean} in fluvial-tidal settings is taken from the Mean Sea-Level (MSL) water elevation.

Tests conducted on data from each zone show that primary dune η, λ, AR, BSI, BRI, and maximum and mean θ_{lee} can be approximated via Gamma distributions (cf. Paola and Borgman, 1991; van der Mark et al., 2008; Cisneros et al., 2020), whilst NDS indices cannot due to the lower number (N) of dunes analysed. Therefore, the zone mean, median, standard deviation, and 25th and 75th quartile values reported herein, for the metrics of η, λ, AR, BSI, BRI, and maximum and mean θ_{lee}, were acquired by applying a Gamma probability density function

(PDF) fit to raw measurements, whilst mean zone NDS values and standard deviations were obtained arithmetically from raw measurements.

4 RESULTS: PRIMARY DUNES

Two categories of primary dunes were recognised in deep fluvial-tidal transition channels (local H/H_{max} ≥ 0.7): i) smaller-scale upstream oriented dunes (~ rkm 1-27; z1-5), and ii) further upstream, larger-scale downstream oriented dunes (~ rkm 34-85; z6-11). In total, ~ 1,400 dunes were analysed, with the number of dunes examined per zone and their morphologic attributes being reported in Table 4 and Figure 12A-F. Below, the average morphology of these two categories of dunes is described within the context of past research as well as: i) varying longitudinal position along the fluvial-tidal transition of the LCR, ii) mean channel depths, and iii) channel bed grain size.

4.1 Upstream oriented dunes: zones 1-5

The z1-5 dunes are positioned within the tidally-dominated regime (~ rkm 1-32) and are composed of fine sand (125-250μm; Figure 3B). The z1 and z2 dunes are likely a mixture of simple and compound forms, whilst those of z3-5 tend to have simple forms (Figure 9; A-A' to E-E'). Topographic profiles in isolation, however, cannot distinguish simple from compound dunes (especially those that are compound and possess superimposed bedforms with η ≥ their host; Dalrymple and Rhodes, 1995). Detailed stratigraphic evidence (i.e., presence of simple *vs* compound cross-bedding) is thus needed to unequivocally confirm whether some of the z1-2 dunes are compound in form (Dalrymple, 1984). Without this information, the z1-5 dunes are considered herein as simple in form following the previous observations of

Sherwood and Creager (1990; Table 1). Overall, z1-5 dunes are relatively small-scale with mean η and λ ranging from ~ 0.3-0.8m and ~ 13-24m (Figure 13), and thus possess mean aspect ratios of ~ 24-68 (Figure 12A, B). They are predominantly 2D (NDS ≤ 1.08), asymmetric (BSIs > 1.5), not rounded (BRIs < 0.6), and possess near equal mean and maximum θ_{lee} (~ 7-11° and ~ 10-15°, respectively; Figure 12C-F). These bedforms are therefore low-angle dunes possessing leesides with relatively mild dipping slip-faces (i.e., lee form 1; Figure 11C), where their mean θ_{lee} is comparable to both sand-bed river and estuarine LADs (≤ 10°, Figure 12F). Overall, they resemble the Type-A and B dunes (Table 1) of Sherwood and Creager (1990), where those of z1 and z2 are interpreted to be tidally-reversing (i.e., Type-A) and those of z3-5 reverse migration direction in response to the fluvial-hydrograph (i.e., Type-B).

Here, scaling of dune η and λ to H_{mean} shows that η/H_{mean} and λ/H_{mean} ratios span ~ 0.02-0.04 and ~ 0.7-1.2, respectively, which fall well below published best fit values for deep rivers and estuaries (Figure 14A, B), and thus plot near, or below, the lower boundary of both tidal and fluvial dunes where η/H_{mean} = 0.025 and λ/H_{mean} = 1.0. Compared to the H_{mean} and channel bed grain size of other rivers, their aspect ratios are relatively small, but plot within, or above, the range of those in estuaries (Figure 14C and D). Lastly, their relatively low maximum θ_{lee} likely causes intermittent flow separation over dune crests, which is consistent with other sand-bed river LADs (i.e., grain size > 125 to ≤ 2000 μm; Figure 14E and F).

4.2 Downstream oriented dunes: zones 6-11

At low-river stage, the mixed tidal-fluvial regime (z6-11; ~ rkm 34-84) begins immediately upstream of the maximum extent of saltwater intrusion during high-river

flows, where bed sediment increases in size to medium to coarse sands (Figure 3B). The first consequence of this shift in hydraulics and grain size is that all primary dunes become seaward-oriented (Figure 9) and larger in size, where average η, λ, and aspect ratios range from ~ 2-3m, ~ 60-110m, and ~ 30-55, respectively (Figure 12A). These values are equivalent to fully-fluvial dunes in the middle Columbia River reported by Smith and McLean (1977), whilst their aspect ratios remain comparable to those of the tidally-dominated regime (Figure 12B). In contrast to the tidally-dominated regime, the larger and coarser-grained dunes of the mixed tidal-fluvial regime (z6-11) are compound in form (Figure 9 F-F' to K-K', and Figure 15), and thus host superimposed bedforms on their crests, stoss-sides, and occasionally their lee-faces. However, similar to the tidally-dominated regime, they tend to be asymmetric (BSIs > 1.5) and not rounded (BRIs < 0.6; Figure 12C and D), but unlike their 2D downstream counterparts, they are mainly 2.5-3D (NDS ≥ 1.08; Figure 12E). According to their mean θ_{lee} (~ 11-18°), dunes of z6-11 are low-angle, but their mean θ_{lee} is marginally steeper than those of the tidally-dominated regime and other river and estuarine settings (Figure 12F). A greater mean θ_{lee} is a consequence of their slip-faces becoming: i) more distinct (i.e., transition in dune lee-side morphology to that of lee form 2A and 2B; Figure 11C) and ii) steeper (maximum θ_{lee} ≈ 18-29°) relative to those of the tidally-dominated regime (Figure 12F). Furthermore, from downstream to upstream, they display a slight increase in both maximum and mean θ_{lee} (z6 to z11; ~ 23-29° and 14-18°; Figure 12F). Overall, the low-angle dunes in the mixed tidal-fluvial regime closely resemble Type-C dunes (Table 1), and those found in other sand-bed rivers (cf. Harbor, 1998; Nittrouer et al., 2008, 2011; Sambrook Smith et al., 2013; de Almeida et al., 2016; Knox and Latrubesse, 2016; Bradley and

Venditti, 2017; Galeazzi et al., 2018; Kostaschuk and Venditti, 2019; Cisneros et al., 2020).

In contrast to the tidally-dominated regime, scaling of mean η and λ to H_{mean} shows that dunes in the mixed tidal-fluvial regime plot along, or very close to, the best fit values for deep rivers where their η/H_{mean} and λ/H_{mean} ratios span 0.12-0.15 and 3.7-6.2 (Figure 14A and B). However, like their finer-grained downstream counterparts, they possess relatively small aspect ratios for a given H_{mean} and grain size, but their aspect ratios tend to be greater than, or equal, to those of estuarine dunes (Figure 14C and D). Comparison of maximum θ_{lee} *vs* H_{mean} and grain size shows that z6-9 dunes possess maximum θ_{lee} values that are steeper than the mean from other sand-bed rivers, and thus likely possess intermittent flow separation over their crests (Figure 14E and F). However, these same relations for z10 and z11 dunes show that their maximum θ_{lee} is notably steeper than most river dunes (regardless of H_{mean}) with similar, or coarser, bed sediment (Figure 14E and F). It is therefore probable that some z10 and z11 dunes can maintain continuous flow separation over their crests, as has been shown for high-angle dunes in shallow rivers and laboratory flumes (Figure 14E and F).

5 DISCUSSION

5.1 Controls on primary dune morphology

Dune morphologic change is a function of how sediment is redistributed by suspended and bedload transport, but more specifically it is the duration of time that a particular transport rate and mode (or q_{sus}/q_{bed} ratio) persists that determines their adjustment (Baas, 1999; Perillo et al., 2014c). Thus, dunes possess a turnover time (i.e., lag time), T_t, which is equal to A/q_s where A is the cross-sectional area of the

dune and q_s is the sediment transport rate per unit width (Myrow et al., 2018). This means that for a constant sediment transport rate and grain size: i) larger dunes possess longer turnover, or development times, relative to smaller dunes, ii) below the transition to an upper flow regime, higher transport rates tend to produce larger dunes over a given time period, and iii) unsteady repetitive flow cycles (i.e., tidal-cycles), and therefore unsteady sediment transport rate and q_{sus}/q_{bed} ratio cycles, produce more rapid morphologic changes in smaller dunes, whilst the constant changes in sediment transport rates and directionality throughout tidal-cycles limits their size.

Within this context, at low-river stage, the deepest (H/H_{max} ≥ 0.7) low-angle dunes of the tidally-dominated regime (z1-5) studied herein are interpreted to be controlled by the twice daily bidirectional tidal-current hysteresis loop that produces cyclic variations in the q_{sus}/q_{bed} ratio of fine to medium sand (125-250μm) due to acceleration and deceleration of ebb- and flood- tidal currents. This loop is characterised by a decrease in the magnitude of dune heights, wavelengths, aspect ratios, and lee-angles, when the q_{sus}/q_{bed} ratio is likely at its highest near peak tidal-velocities, but these characteristics recover as the q_{sus}/q_{bed} ratio, and therefore suspended-sediment concentrations, lowers during the phase shift between ebb- and flood- tidal flows (see figure 6, Hendershot et al., 2016). Thus, the spatio-temporal unsteadiness of flow, sediment transport rates, and the q_{sus}/q_{bed} ratio, restricts the traction-load renourishment of these dunes to a short time window during the waning stages of ebb- and flood- tidal flows when currents are decelerating and formerly intermittently suspended sand is reincorporated into bedload transport (e.g., Sherwood and Creager, 1990; Oost and Baas, 1994). This short renourishment window prevents their heights and wavelengths from reaching

values that scale to mean flow depths (cf. Baas, 1999; Perillo et al., 2014c), impedes lee-angles from steepening towards the angle-of-repose, and promotes the creation of simple forms that are 2D (e.g., Baas, 1994, 1999; Dalrymple and Rhodes, 1995; Venditti et al., 2005a; Rubin, 2012). Secondarily, the suppression of their heights and wavelengths is also likely augmented by flow stratification, and thus restriction of boundary layer thickness, caused by either saltwater intrusion or high nearbed suspended-sediment concentrations during peak tidal-current velocities (Jay and Smith, 1990; Dalrymple and Rhodes, 1995; Kay and Jay, 2003).

During low-river stages, however, the tidal hysteresis loop of cyclic q_{sus}/q_{bed} ratios is not equal spatially from z1 to z5, due to the upstream development of tidal-current asymmetry at depths where H/H_{max} > 0.5 (i.e., flood-tidal currents become stronger than ebb-tidal currents towards z5 as a product of saltwedge density-stratification and tidal-funnelling; Jay, 1984; Jay and Smith, 1990), and a slight coarsening of the channel bed. Thus, within z1 and z2, hysteresis loops in the ebb- and flood- tidal cycle q_{sus}/q_{bed} ratio may be more symmetric and higher in magnitude, which leads to higher q_{bed} of fine to medium sand during the waning stages of tidal-phases and thus larger dune heights. In comparison, the ebb- and flood- current hysteresis loop in q_{sus}/q_{bed} ratio will become increasing asymmetric (the flood-tidal phase becomes more dominant) from z3 to z5, although their overall magnitude will be weaker. This causes lower q_{bed} of fine to medium sand during the waning stages of tidal-phases, and consequently leads to smaller dune heights. Together, these factors are reasoned to cause the downstream to upstream trend in decreasing dune height from z1 to z5 and the switch from migration reversing during the tidal-cycle (z1 and z2) to upstream-only migration (z3-5; Figure 4A). Furthermore, the overall greater rate of tidally-induced intermittent sand suspension

(higher q_{sus}/q_{bed} ratios) throughout z1-5 is reasoned to be the principal mechanism driving these simple dunes to possess low (and nearly equivalent) maximum and mean lee-angles (i.e., lee form 1 morphology, Figure 11C), or gentle sloping slip-faces (e.g., Smith and McLean, 1977; Bridge and Best, 1988; Kostaschuk and Villard, 1996; Kostaschuk et al., 2009; Hendershot et al., 2016; Bradley and Venditti, 2017; Ma et al., 2017; Naqshband and Hoitink, 2020).

At low-river stage, the morphology of the larger and coarser-grained (250-750μm) low-angle dunes of the mixed tidal-fluvial regime (z6-11) is interpreted to be a function of a seasonally varying hysteresis loop involving: i) a first stage dominated by unidirectional currents at high-river flows, and ii) a second governed by bidirectional tidal-currents during subsequent low-river flows. Through time, the first stage is responsible for establishing and maintaining dunes of a larger size and with downstream-orientations, because peak fluvial-discharges commonly last up to 3-4 months and are typically ~ 2.5 to 4 times larger than low-flow discharges (Table 2; Fig. 2A). These greater flows generate considerably greater suspended and bedload transport rates since the discharge-sediment rating curve of the LCR takes the form of a power-law (Naik and Jay, 2011). These higher transport rates (especially bedload transport) will thus enhance the rates of primary dune migration and growth (Baas, 1999; Perillo et al., 2014c), which in turn promotes greater crestline sinuosity or dimensionality (2.5-3D; e.g., Baas, 1994, 1999; Dalrymple and Rhodes, 1995; Venditti et al., 2005a; Rubin, 2012), and the development of superimposed bedforms on their stoss-sides thus producing a compound form. However, although not universally agreed upon, their compound forms may be aided by the fact that their grain size is near or above an observed threshold of ≥ 274μm for compound dune formation (Jackson 1976; Dalrymple 1984; Dalrymple and Rhodes, 1995; Bartholdy

et al., 2002). Additionally, greater q_{sus} in conjunction with superimposed bedform migration and growth, will tend to generate shallower leeside angles (e.g., Dalrymple and Rhodes, 1995; Carling et al., 2000; Sukhodolov et al., 2006; Reesink and Bridge, 2009; Naqshband and Hoitink, 2020). Furthermore, according to the numerical simulations of Sandbach et al. (2018), high fluvial-flows in the LCR eliminate current reversals induced by the flood-tide throughout z6-11, thus leaving seaward-oriented currents as the principal driver of dune morphodynamics. Together, the above factors provide a rationale as to why many of the geometric characteristics of dunes in z6-11 closely resemble those of the middle Columbia River, or in general, those in fully-fluvial settings of similar grain size.

Although the morphology of z6-11 compound dunes is reasoned to be largely the product of strong downstream-oriented currents at high-river stage in conjunction with their coarser grain size, the 8-9 month long low-river stage period of the hysteresis loop (i.e., lower overall sediment transport rates operating over a longer duration of time) is interpreted to impact the relict high-flow dunes in three ways. First, bidirectional tidal-currents, and perhaps especially ebb-currents, likely promote the development of new superimposed bedforms, or sustain previously existing ones, thus helping to maintain their compound form. Secondly, superimposed bedforms likely suppress flow separation over their host dunes and rework their crests, leesides, and stoss-sides, which helps to maintain their lower mean lee-angles (e.g., Allen and Collinson, 1974; Allen, 1978; Dalrymple and Rhodes, 1995; Carling et al., 2000; Sukhodolov et al., 2006; Reesink and Bridge, 2009; Best et al., 2020; Cisneros et al., 2020). Thirdly, the slight downstream to upstream increase in dune heights from z6 to z11 (Figure 12A) is reasoned to be the product of the

lessening potential of superimposed bedforms to rework sediment as a function of decreasing tidal-current energy and the coarsening of bed alluvium (Figure 3B).

Several findings from the present study contrast with previous research concerning dune morphodynamics. Firstly, the compound low-angle dunes of the mixed tidal-fluvial regime (i.e., dominated by downstream oriented currents) are asymmetric and not rounded, whilst a large percentage of the upstream most dunes (z10 and z11) likely display continuous flow separation (i.e., maximum lee-angles > 25°). Their asymmetry and lack of roundness thus makes them distinct from those in rivers, but similar to those in estuaries (Dalrymple and Rhodes, 1995; Bradley and Venditti, 2017), whereas the likely continuous flow separation over the z10 and z11 dunes contrasts with that in many river and estuarine settings. This suggests that: i) dune asymmetry and absence of roundness may be an indicator of tidal-forcing within the mixed fluvial-tidal regime of fluvial-tidal transitions, and ii) some low-angle dunes may sustain continuous flow separation over their crests (Cisneros et al., 2020). However, further research is necessary to confirm whether these observations are universal, or restricted to the Lower Columbia River. Secondly, at low-river stage, there is a downstream to upstream trend (i.e., tidally-dominated to mixed tidal-fluvial regime) in the steepening of dune maximum and mean lee-angles, as well as a shift in leeside morphology (from lee form 1 to lee form 2A and B; Figure 11C).

This trend is reasoned to be the product of the downstream to upstream: i) coarsening of channel bed grain size and thus a decrease in q_{sus}/q_{bed} ratios (i.e., bedload transport becomes more dominant in landward direction), and ii) reduction in the reworking of compound dunes by superimposed bedforms throughout the mixed tidal-fluvial regime, caused by the decrease in tidal-current energy. This condition is

likely enhanced in the Lower Columbia River since ≥ 50% of sand-sized grains are heavy minerals (specific gravity ≥ 2.8; Whetten et al., 1969; Scheidegger and Phipps, 1976) that will possess a different hydraulic equivalence to lighter minerals such as quartz and feldspar. Therefore, for a given bed shear stress, the LCR possesses a lower q_{sus}/q_{bed} ratio (i.e., more bedload transport dominated) than systems whose sand-grade sediment consists of less dense grains of quartz and feldspar. Because higher q_{sus}/q_{bed} ratios reduce lee-angles (cf. Best and Kostaschuk, 2002; Hendershot et al., 2016; Kostaschuk and Venditti, 2019; Cisneros et al., 2020; Naqshband and Hoitink, 2020), it is unsurprising that the steepest lee-angles (lee form 2A or B) occur in the coarsest grained regions of the upper mixed tidal-fluvial regime (z10 and z11) where q_{sus}/q_{bed} ratios are presumably the lowest at low-river stages. Lower overall q_{sus}/q_{bed} ratios may also help to explain why the low-angle dunes of the LCR fluvial-tidal transition tend to be more asymmetric and not rounded, similar to the high-angle dunes of sand-bed shallow rivers and flumes. Although progress has been made in understanding the effects of grain density on sediment sorting (for example, Viparelli et al., 2015), more research is needed to fully understand the effects of variable mineral density on bedform morphology. Additionally, during low-river stages, it is unlikely that the upstream trend in decreasing q_{sus}/q_{bed} ratios is exclusive to the LCR, suggesting that all sand-bed fluvial-tidal transitions displaying downstream fining trends may possess a landward steepening in primary dune lee-angles, and thus also their cross-bed dip-angles.

5.3 Implications of trends in dune morphology

During low-river stages, ~ 86% of the deepest (H/H_{max} ≥ 0.7) channel bed of the Lower Columbia River fluvial-tidal transition is populated by larger-scale primary dunes that are compound and possess seaward orientations, and therefore are more 'fluvial' in their character, whilst ~ 90% is populated by such dunes during high-river stages (see Sherwood & Creager, 1990; Figure 16A, B). Thus, only the most-seaward main channel of the fluvial-tidal transition (maximum of ~ 14% of total) displays smaller-scale, simple dunes with spatio-temporally fluctuating orientations indicative of a 'fluvial-tidal to tidal' signature (Figure 16A, B). Overall, this large-scale morphological pattern is more comparable to a tidally-influenced fluvio-deltaic environment, rather than a tidally-dominated estuary, which supports the findings of Prokocki et al. (2015, 2020). Furthermore, the downstream to upstream trend of increasing dune size through its fluvial-tidal transition at low-river stage suggests an accompanying upstream-directed increase in their form drag. Seasonal variations in the fluvial hydrograph, however, complicate this pattern by generating a localised 'dynamic morphology reach' extending from ~ rkm 12-35, where dunes experience the greatest spatio-temporal variation in morphology, due to the down-river expansion and contraction of hydraulic regimes, associated changes in the extent of saltwater intrusion, and variations in channel bed grain size (Figure 16A, B).

For instance, at high-river stage, there is a seaward expansion of coarser grained 'fluvial' dunes from ~ rkm 35 to 27, and a 180° reversal in orientation (from upstream to downstream directed) of the smaller-scale 'fluvial-tidal' dunes between ~ rkm 12-21. However, during the following low-river stage, tidal-energy (especially flood-tidal energy and saltwater intrusion) penetrates further upstream causing the 'fluvial-tidal' dunes between ~ rkm 12-21 to reverse their orientation by 180°

(downstream to upstream) and to extend their development upstream to ~ rkm 32 via (Figure 16A,B): i) cannibalisation of previously existing high-river stage 'fluvial' dunes between ~ rkm 27-32, and/or ii) fining of channel bed alluvium below the possible grain-size limit necessary to form the coarser 'fluvial' dunes. These morphological fluctuations will inevitably generate variations in the magnitude of form drag within the 'dynamic morphology reach', which should thus be parameterised for incorporation into hydraulic and morphodynamic simulations (Unsworth et al., 2020). Moreover, relative to those dunes positioned farther downstream or upstream, the style, thickness, and orientation of the deposits of primary dunes within the 'dynamic morphology reach' likely show the greatest variance, switching between upstream and downstream oriented, simple to compound, cross-bedding whose cross-sets will vary from thinner to thicker. These unique cross-bed sets may represent a distinct sedimentological signature to use when evaluating evidence of deltaic fluvial-tidal transitions or river dominated reaches of estuarine fluvial-tidal transitions in ancient fluvio-tidal environments that possess a similar downstream fining trend as the Lower Columbia River.

6 CONCLUSIONS

The deepest (H/H_{max} ≥ 0.7) channels of the Lower Columbia River, and likely other deltaic fluvial-tidal transitions and river-dominated reaches of estuarine fluvial-tidal transitions with similar downstream fining trends and hydraulic characteristics, are dominated by low-angle primary dunes. The height of these dunes, and thus form drag, may abruptly increase landward of the extent of salinity intrusion during high-river stage or within the mixed tidal-fluvial hydraulic regime at low-river stage. In these fluvial-tidal transitions, seaward-directed currents tend to control dune

morphology, whilst the effects of bidirectional tidal-flows are subordinate. Thus, at depths where H/H_{max} ≥ 0.7, up to 90% of their thalwegs will possess 'fluvial' low-angle dunes (medium to coarse sand, large-scale, 2.5-3D, downstream-oriented, and compound) whose morphology is very similar to those in sand-bed rivers. Only the most seaward thalweg reaches (< *c*. 20% of their total longitudinal extent), where H/H_{max} ≥ 0.7, will display 'fluvial-tidal or tidal' low-angle dunes (smaller-scale, 2D, and simple or compound?) composed of fine sand with reversing orientations caused by tidal-cycles and/or fluctuations in fluvial-discharge. The low-angle character of the most seaward 'fluvial-tidal or tidal' dunes are likely the product of higher suspended-sediment transport, q_{sus}, relative to bedload sediment transport, q_{bed}, over tidal-cycles. Alternatively, the upstream 'fluvial' dunes, where q_{sus}/q_{bed} ratios are generally lower, owe their low-angle character to reworking of their crests, stoss-sides, and leesides via the migration and development of superimposed bedforms during both low- and high- river stages, and likely higher q_{sus} during high-discharge periods.

Primary low-angle dunes display a downstream (maximum lee-angle ~ 11-15°; mean lee-angle ~ 7-11°) to upstream (maximum lee-angle ~ 18-29°; mean lee-angle ~ 11-18°) steepening trend through the fluvial-tidal transition of the LCR. This trend suggests that: i) their cross-bed dip-angles may also steepen, and ii) a greater proportion will transition from those with intermittent flow separation (maximum lee-angles ≥ 10 to ≤ 25°) to those displaying continuous flow separation (maximum lee-angles > 25°). This trend may exist at low-river stages in all upstream-coarsening (i.e., fine to coarse/medium sand) deltaic fluvial-tidal transitions and river-dominated portions of estuarine fluvial-tidal transitions and is potentially a signature of their fluvial-tidal transition. Fluctuations in discharge of the Lower Columbia River create a

‘dynamic morphology reach’ within the thalweg (H/H_{max} ≥ 0.7) of its fluvial-tidal transition, which displays the greatest morphological variability in primary dunes, and thus associated form drag. If the Lower Columbia River provides a case study that can be applied to other similar environments, these variations in form drag must be incorporated into hydraulic or morphodynamic simulations of such fluvial-tidal transitions. These deviations in dune morphology also likely cause the style, thickness, and orientation of stacked dune cross-sets at or near deep channel bases to possess the greatest variations relative to seaward and landward channel locations and may provide a criterion for recognition of these environments in ancient sedimentary sequences.

REFERENCES

Aliotta S, Perillo, GME. 1987. A sand wave field in the entrance to Bahía Blanca estuary, Argentina. *Marine Geology* 76: 1-14.

Allen JRL. 1968. Current Ripples: Their Relation to Patterns of Water and Sediment Motion. *North-Holland Pub., Amsterdam*: 433 p.

Allen JRL. 1974. Reaction, relaxation and lag in natural sedimentary systems: general principles, examples and lessons. *Earth Science Reviews* 10(4): 263-342.

Allen JRL. 1976. Time-lag of dunes in unsteady flows: an analysis of Nasner's data from the River Weser, Germany. *Sedimentary Geology* 15(4): 309-321.

Allen JRL. 1978. Polymodal dune assemblages: an interpretation in terms of dune creation-destruction in periodic flows. Sedimentary Geology 20: 17-28.

Allen JRL. 1982. Sedimentary Structures: Their Character and Physical Basis, Volumes 1 and 2. *Elsevier, Amsterdam*: 593 p.

Allen JRL. 1983. River bedforms: progress and problems. In Modern and Ancient Fluvial Systems, Collinson J, Lewin J (eds.). *International Association of Sedimentologists, Special Publication* 6: 19-33.

Allen JRL, Collinson JD. 1974. The superimposition and classification of dunes formed by unidirectional aqueous flows. Sedimentary Geology 12: 169-178.

Amsler ML, Schreider MI. 1999. Dune height prediction at floods in the Paraná river, Argentina. In River Sedimentation: Theory and Applications, Jayewardena JHW, Wang L, Wang Y. (eds.). A.A. Balkema, Brookfield, VT: 615-620.

Arnott RW, Southard JB. 1990. Exploratory flow-duct experiments on combined-flow bed configurations, and some implications for interpreting storm event stratification. *Journal of Sedimentary Petrology* 60: 211-219.

Ashley GM. 1990. Classification of large-scale subaqueous bedforms: a new look at an old problem. *Journal of Sedimentary Petrology* 60(1): 160-172.

Baas JH. 1994. A flume study on the development and equilibrium morphology of current ripples in very fine sand. *Sedimentology* 41: 185-209.

Baas JH. 1999. An empirical model for the development and equilibrium morphology of current ripples in fine sand. *Sedimentology* 46(1): 123-138.

Barnard PL, Erikson LH, Kvitek RG. 2011. Small-scale sediment transport patterns and bedform morphodynamics: new insights from high-resolution multibeam bathymetry. *Geo-Marine Letters* 31: 227-236.

Bartholdy J, Bartholomae A., Flemming BW. 2002. Grain-size control of large compound flow-transverse bedforms in a tidal inlet of the Danish Wadden Sea. *Marine Geology* 188: 391-413.

Best JL. 2005. The fluid dynamics of river dunes: A review and some future research directions. *Journal of Geophysical Research* 110: F04S02. doi:10.1029/2004JF000218.

Best JL, Fielding CR. 2019. Describing fluvial systems: linking processes to deposits and stratigraphy. In *River to Reservoir: Geoscience to Engineering, Geological Society of London Special Publication* 488: 152-166.

Best JL, Kostaschuk R. 2002. An experimental study of turbulent flow over a low-angle dune. *Journal of Geophysical Research* 107: 3135. doi:10.1029/2000JC000294.

Best J, Cisneros J, Almeida RP, Galaezzi C, Ianniruberto M, Ma H, Unsworth C, van Dijk T. 2020. Why do large, deep rivers have low-angle dune beds?: *Comment, Geology* 48: e50. https://doi.org/10.1130/G47578C.1

Blasius H. 1910. Über die Abhängigkeit der Formen der Riffeln and Geschiebebänke vom Gefälle. *Zeitschrift für Bauwesen* 60: 466-472.

Bradley RW, Venditti JG. 2017. Reevaluating dune scaling relations. *Earth Science Reviews* 165: 356-376.

Bradley RW, Venditti JG. 2019a. Transport scaling of dune dimensions in shallow flows. *Journal of Geophysical Research: Earth Surface* 124: 526-547. https://doi.org/10.1029/2018JF004832.

Bradley RW, Venditti JG. 2019b. The growth of dunes in rivers. *Journal of Geophysical Research: Earth Surface* 124: 548-566. https://doi.org/10.1029/2018JF004835.

Bradley RW, Venditti JG, Kostaschuk RA, Church M, Hendershot M, Allison MA. 2013. Flow and sediment suspension events over low angle dunes: Fraser Estuary, Canada. *Journal of Geophysical Research: Earth Surface* 118. doi:10.1002/jgrf.20118.

Bridge JS. 2003. Rivers and Floodplains: Forms, Processes, and Sedimentary Record. Blackwell Publishing, Oxford, UK.

Bridge JS, Best JL. 1988. Flow, sediment transport and bedform dynamics over the transition from dunes to upper-stage plane beds: implications for the formation of planar laminae. *Sedimentology* 35: 753-763.

Carle L, Hill PR. 2009. Subaqueous dunes of the upper slope of the Fraser River Delta (British Columbia, Canada). *Journal of Coastal Research* 25(2): 448-458.

Carling PA, Golz E, Orr HG, Radecki-Pawlik A. 2000. The morphodynamics of fluvial sand dunes in the river Rhine near Mainz, Germany, part I: sedimentology and morphology. *Sedimentology* 47: 227-252.

Chawla A, Jay DA, Baptista AM, Wilkin M, Seaton C. 2008. Seasonal variability and estuary-shelf interactions in circulation dynamics of a river-dominated estuary. *Estuaries and Coasts* 31: 269-288.

Cisneros J, Best J, van Dijk T, de Almeida RP, Amsler M, Boldt J, Freitas B, Galeazzi, C, Huizinga R, Iannirubertо M, Ma H, Nittrouer JA, Oberg K, Orfeo O, Parsons D, Szupiany R, Wang P, Zhang Y. 2020. Dunes in the world's big rivers are characterized by low-angle lee-slopes and a complex shape. *Nature Geoscience* 13: 156-162.

Clark SM, Snyder GR. 1969. Timing and extent of flow reversal in the lower Columbia River. *Journal of Limnology and Oceanography* 14: 960-965.
Dalrymple RW. 1984. Morphology and internal structure of sandwaves in the Bay of Fundy. *Sedimentology* 31: 365-382.

Dalrymple RW, Choi K. 2007. Morphologic and facies trends through the fluvial-marine transition in tide-dominated depositional systems: A schematic framework for environmental and sequence-stratigraphic interpretation. *Earth Science Reviews* 81: 135-174.

Dalrymple RW, Rhodes RN. 1995. Estuarine dunes and bars. In Geomorphology and Sedimentology of Estuaries, Perillo GME. (eds.). *Developments in Sedimentology* 53: 359-422.

Dalrymple RW, Knight RJ, Lambiase JJ. 1978. Bedforms and their hydraulic stability relationships in a tidal environment, Bay of Fundy, Canada. *Nature* 275: 100-104.

Dalrymple RW, Kurcinka CE, Jablonski BVJ, Ichaso AA, Mackay DA. 2015. Deciphering the relative importance of fluvial and tidal processes in the fluvial-marine transition. In Fluvial-Tidal Sedimentology, Ashworth PJ, Best JL, Parsons DR. (eds.). *Developments in Sedimentology* 68: 3-45.

Davis RA Jr, Flemming BW. 1991. Time-series study of mesoscale tidal bedforms, Martens Plate, Wadden Sea, Germany. In Clastic Tidal Sedimentology, Smith DG, Reinson GE, Zaitlin BA, Rahmani RA (eds.). *Canadian Society of Petroleum Geology Memoir* 16: 275-282.

de Almeida RP, Galeazzi CP, Freitas BT, Janikian L, Iannirubertо M, Marconato A. 2016. Large barchanoid dunes in the Amazon River and the rock record: Implications for interpreting large river systems. *Earth and Planetary Science Letters* 454: 92-102.

Doucette JS, O'Donoghue T. 2006. Response of sand ripples to change in oscillatory flow. *Sedimentology* 53: 581-596.

Du Buat P. 1786. Principes d'Hydraulique. *De l'Imprimerie de Monsieur* : 453 p.

Dumas S, Arnott R, Southard JB. 2005. Experiments on oscillatory-flow and combined-flow bedforms: implications for interpreting parts of the shallow-marine sedimentary record. *Journal of Sedimentary Research* 75: 501-513.

Elliot T, Gardiner AR. 1981. Ripple, megaripple and sandwave bedforms in the macrotidal Loughor estuary, south Wales, UK. In Holocene Marine Sedimentation in the North Sea Basin, Nio SD, Shüttenhelm RTE, van Weering TJCE (eds.). *International Association of Sedimentologists Special Publication* 5: 51-64.

Ernstsen VB, Winter C, Becker M, Bartholdy J. 2010. Tide-controlled variations of primary-and secondary-bedform height: Innenjade tidal channel (Jade Bay, German Bight). In River, Coastal and Estuarine Morphodynamics: RCEM 2009, Vionnet C, Perillo G, Latrubesse E, Garcia M. (eds.): 779-786.

Fain AMV, Jay DA, Wilson DJ, Orton PM, Baptista AM. 2001. Seasonal and tidal monthly patterns of particulate matter dynamics in the Columbia River estuary. *Estuaries* 24(5): 770-786.

Fox DS, Bell S, Nehlsen W, Damron J. 1984. The Columbia River Estuary: atlas of physical and biological characteristics. Columbia River Data Development Program (CREDDP), Astoria, OR: 87p.

Fraccascia S, Winter C, Ernstsen VB, Hebbeln D. 2016. Residual currents and bedform migration in a natural tidal inlet (Knudedyb, Danish Wadden Sea). *Geomorphology* 271: 74-83.

Galeazzi CP, Almeida RP, Mazoca CEM, Best JL, Freitas BT, Ianniruberto M, Cisneros, J, Tamura LN. 2018. The significance of superimposed dunes in the Amazon River: Implications for how large rivers are identified in the rock record. *Sedimentology* 65(7): 2388-2403. doi.org/10.1111/sed.12471.

Gelfenbaum G. 1983. Suspended-sediment response to semidiurnal and fortnightly tidal variations in a mesotidal estuary: Columbia River, USA. *Marine Geology* 52: 39-57.

Gelfenbaum G, Sherwood CR, Peterson CD, Kaminsky GM, Buijsman M, Twichell DC, Ruggiero P, Gibbs AE, Reed C. 1999. The Columbia River littoral cell - a sediment budget overview. In Coastal Sediments '99, Long Island, NY, 1999, *Proceedings American Society of Civil Engineers*: 1660-1675.

Giese BS, Jay DA. 1989. Modelling tidal energetics of the Columbia River Estuary. *Estuarine, Coastal and Shelf Science* 29: 549-571.

Gómez EA, Cuadrado DG, Pierini JO. 2010. Sand transport on an estuarine submarine dune field. *Geomorphology* 121: 257-265.

Guerrero M, Lamberti A. 2011. Flow field and morphology mapping using ADCP and multibeam techniques: Survey in the Po River. *Journal of Hydraulic Engineering* 137(12): 1576-1587.

Hamilton P. 1990. Modelling salinity and circulation for the Columbia River estuary. *Progress in Oceanography* 25: 113-156.

Harbor DJ. 1998. Dynamics of bedforms in the Lower Mississippi River. *Journal of Sedimentary Research* 68(5): 750-762.

Harms JC. 1969. Hydraulic significance of some sand ripples. *Geological Society of America Bulletin* 80: 363-396.

Harms JC, Southard JB, Spearing D, Walker R. 1975. Depositional Environments as Interpreted from Primary Sedimentary Structures and Stratification Sequences. *Society of Economic Paleontologists and Mineralogists, Short Course 2*: 161 p.

Harris PT. 1988. Large-scale bedforms as indicators of mutually evasive sand transport and the sequential infilling of wide-mouthed estuaries. *Sedimentary Geology* 57: 273-298.

Hendershot ML, Venditti JG, Bradley RW, Kostaschuk RA, Church M, Allison MA. 2016. Response of low-angle dunes to variable flow. *Sedimentology* 63: 743-760.

Hickson RE. 1912. A report on the establishment of river gauges on lower Columbia River & Willamette Rivers. Report to the US Army Corps of Engineers.

Hoitink AJF, Jay DA. 2016. Tidal river dynamics: Implications for deltas. *Reviews of Geophysics* 54: 240-272.

Holmes RR, Garcia MH. 2008. Flow over bedforms in a large sand-bed river: a field investigation. *Journal of Hydraulic Research* 46: 322-333. doi:10.3826/jhr.2008.3040.

Hughes FW, Rattray Jr. M. 1980. Salt flux and mixing in the Columbia River estuary. *Estuarine and Coastal Marine Science* 10: 479-493.

Jackson RG. 1976. Large scale ripples of the lower Wabash River. *Sedimentology* 23: 593-623.

Jay DA. 1984. Circulatory processes in the Columbia River Estuary. Astoria, OR, CREST: 169p.

Jay DA, Smith JD. 1990. Circulation, density distribution and neap-spring transitions in the Columbia River Estuary. *Progress in Oceanography* 25: 81-112.

Jay DA, Giese BS, Sherwood CR. 1990. Energetics and sedimentary processes in the Columbia River Estuary. *Progress in Oceanography* 25: 157-174.

Kay DJ, Jay DA. 2003. Interfacial mixing in a highly-stratified estuary 2. A method of constrained differences approach for the determination of the momentum and mass

balances and the energy of mixing. *Journal of Geophysical Research* 108: C3, 3073. doi:10/1029/2000JC000253

Kennedy JF. 1969. The formation of sediment ripples, dunes, and antidunes. *Annual Review of Fluid Mechanics* 1: 147-168.

Kleinhans MG. 2001. The key role of fluvial dunes in transport and deposition of sand-gravel mixtures, a preliminary note. *Sedimentary Geology* 143: 7-13.

Knox RL, Latrubesse EM. 2016. A geomorphic approach to the analysis of bedload and bed morphology of the Lower Mississippi River near the Old River Control Structure. *Geomorphology* 268: 35-47.

Kostaschuk RA, Venditti JG. 2019. Why do large, deep rivers have low-angle dune beds? *Geology* 47: 919-922. doi.org/10.1130/G46460.1.

Kostaschuk RA, Villard PV. 1996. Flow and sediment transport over large subaqueous dunes: Fraser River, Canada. *Sedimentology* 43: 849-863.

Kostaschuk RA, Villard PV. 1999. Turbulent sand suspension over dunes. In Fluvial Sedimentology VI, Smith N.D. and Rogers J. (eds.) *International Association of Sedimentologists Special Publication* 28: 3-14.

Kostaschuk RA, Shugar D, Best J, Parsons D, Lane S, Hardy R, Orfeo O. 2009. Suspended sediment transport and deposition over a dune: Rio Paraná, Argentina. *Earth Surface Processes and Landforms* 34: 1605-1611.

Kukulka T, Jay DA. 2003. Impacts of Columbia River discharge on salmonoid habitat: 1. A nonstationary fluvial tide model. *Journal of Geophysical Research* 108(C9): 3293. doi:10.1029/2002JC001382.

Langhorne DN. 1973. A sandwave field in the outer Thames estuary, Great Britain. *Marine Geology* 14: 129-143.

Lefebvre A. 2019. Three-dimensional flow above river bedforms: insights from numerical modelling of a natural dune field (Rio Parana, Argentina). *Journal of Geophysical Research: Earth Surface* 124: 2241-2264. doi:10/1029/2018JF004928.

Lefebvre A, Winter C. 2016. Predicting bed form roughness: the influence of lee side angle. *Geo-Mar. Lett.* 36: 121-133. doi:10.1007/s00367-016-0436-8

Lefebvre A, Ernstsen VB, Winter C. 2011. Influence of compound bedforms on hydraulic roughness in a tidal environment. *Ocean Dynamics* 61: 2201-2210.

Lefebvre A, Paarlberg A, Winter C. 2014a. Flow separation and shear stress over angle-of-repose bedforms: a numerical investigation. *Water Resources Research* 50: 986-1005. doi:10.1002/2013WR014587.

Lefebvre A, Paarlberg AJ, Ernstsen VB, Winter C. 2014b. Flow separation and roughness lengths over large bedforms in a tidal environment: a numerical investigation. *Continental Shelf Research* 91: 57-69.

Ma H, Nittrouer JA, Naito K, Fu X., Zhang Y, Moodie AJ, Wang Y, Wu B, Parker G. 2017. The exceptional sediment load of fine-grained dispersal systems: example of the Yellow River, China. *Science Advances* 3: e1603114.

Martin RL, Jerolmack DJ. 2013. Origin of hysteresis in bed form response to unsteady flows. *Water Resources Research* 49: 1314-1333.

Martinius AW, Van den Berg JH. 2011. Atlas of sedimentary structures in estuarine and tidally-influenced river deposits of the Rhine-Meuse-Scheldt system: their application to the interpretation of analogous outcrop and subsurface depositional systems. EAGE Publications, Houten, The Netherlands: 298p.

Mei X, Dai Z, Darby SE, Zhang M, Cai H, Wang J. 2021. Landward shifts of the maximum accretion zone in the tidal reach of the Changjiang estuary following construction of the Three Gorges Dam. *Journal of Hydrology* 592: 125789. https://doi.org/10.1016/j.jhydrol.2020.125789

Myrow PM, Southard JB. 1991. Combined-flow model for vertical stratification sequences in shallow marine storm-deposited beds. *Journal of Sedimentary Petrology* 61: 202-210.

Myrow PM, Fischer W, Goodge JW. 2002. Wave-modified turbidites: combined-flow shoreline and shelf deposits, Cambrian, Antarctica. *Journal of Sedimentary Research* 72: 641-656.

Myrow PM, Jerolmack DJ, Perron JT. 2018. Bedform disequilibrium. *Journal of Sedimentary Research* 88: 1096-1113.

Naik PK, Jay DA. 2011. Distinguishing human and climate influences on the Columbia River: Changes in mean flow and sediment transport. *Journal of Hydrology* 404: 259-277.

Naqshband S, Hoitink AJF. 2020. Scale-dependent evanescence of river dunes during discharge extremes. *Geophysical Research Letters* 47: *e2019GL085902*. https://doi.org/10.1029/2019GL085902

Neal VT. 1972. Physical aspects of the Columbia River and its estuary. In *The Columbia River Estuary and Adjacent Ocean Waters*, Pruter AT, Alverson DL. (eds.), University of Washington Press, Seattle, Washington: 40p.

Nittrouer JA, Allison MA, Campanella R. 2008. Bedform transport rates for the lowermost Mississippi River. *Journal of Geophysical Research* 113: F03004. doi:10.1029/2007JF000795.

Nittrouer JA, Mohrig D, Allison M. 2011. Punctuated sand transport in the lowermost Mississippi River. *Journal of Geophysical Research* 116: F04025. doi:10.1029/2011JF002026.

Oost AP, Baas JH. 1994. The development of small scale bedforms in tidal environments: an empirical model for unsteady flow and its applications. *Sedimentology* 41: 883-903.

Paola C, Borgman L. 1991. Reconstructing random topography from preserved stratification. *Sedimentology* 38: 553-565.

Parsons DR, Best JL. 2013. Bedforms: views and new perspectives from the third international workshop on Marine and River Dune Dynamics (MARID3). *Earth Surface Processes and Landforms* 38: 319-329.

Parsons DR, Best JL, Orfeo O, Hardy RJ, Kostaschuk R, Lane SN. 2005. Morphology and flow fields of three-dimensional dunes, Rio Parana, Argentina: Results from simultaneous multibeam echo sounding and acoustic Doppler current profiling. *Journal of Geophysical Research* 110: F04S03. doi:10.1029/2004JF000231.

Perillo MM. 2013. Flow, sediment transport and bedforms under combined-flows [Ph.D. thesis]. University of Illinois at Urbana-Champaign, 296 p.

Perillo MM, Best JL, Garcia MH. 2014a. A new phase diagram for combined-flow bedforms. *Journal of Sedimentary Research* 84: 301-313.

Perillo MM, Prokocki EW, Best JL, Garcia MH. 2014b. Bedform genesis from bed defects under unidirectional, oscillatory, and combined flows. *Journal of Geophysical Research - Earth Surface* 119: 2635-2652.

Perillo MM, Best JL, Yokokawa M, Sekiguchi T, Takagawa T, Garcia MH. 2014c. A unified model for bedform development and equilibrium under unidirectional, oscillatory, and combined-flows. *Sedimentology* 61: 2063-2085.

Peterson C, Scheidegger K, Komar P, Niem W. 1984. Sediment composition and hydrography in six high-gradient estuaries of the northwestern United States. *Journal of Sedimentary Petrology* 54: 86-97.

Peterson CD, Gates EB, Minor R, Baker DL. 2013. Accommodation space controls on the latest Pleistocene and Holocene (16-0 ka) sediment size and bypassing in the Lower Columbia River Valley: a large fluvial-tidal system in Oregon and Washington, USA. *Journal of Coastal Research* 29(5): 1191-1211.

Peterson C, Vanderburgh S, Roberts MC. 2014. Late Holocene geomorphology of the Columbia River estuary, Oregon and Washington, USA. *Journal of Geography and Geology* 6(2): 1-27.

Prokocki EW, Best JL, Ashworth PJ, Parsons DR, Sambrook Smith GH, Nicholas AP, Simpson CJ, Wang H, Sandbach SD, Keevil CE. 2015. Mid to late Holocene geomorphological and sedimentological evolution of the fluvial-tidal zone: Lower

Columbia River, WA/OR, USA. In *Fluvial-Tidal Sedimentology*, Ashworth PJ, Best JL, Parsons DR. (eds.). *Developments in Sedimentology* 68: 193-226.

Prokocki EW, Best JL, Ashworth PJ, Sambrook Smith GH, Nicholas AP, Parsons DR, Simpson CJ. 2020. Alluvial architecture of mid-channel fluvial-tidal barforms: the mesotidal Lower Columbia River, Oregon/Washington, USA. *Sedimentology* 67: 3533-3566.

Reesink AJ, Bridge J. 2009. Influence of bedform superimposition and flow unsteadiness on the formation of cross strata in dunes and unit bars. Part 2, further experiments. *Sedimentary Geology* 222: 274-300.

Reynaud JY, Dalrymple RW. 2012. Shallow-marine tidal deposits. In Principles of Tidal Sedimentology, Davis Jr. RA, Dalrymple RW. (eds.). Springer, Dordrecht, 335-369.

Rubin DM. 2012. A unifying model for planform straightness of ripples and dunes in air and water. *Earth Science Reviews* 113: 176-185.

Sambrook Smith GH, Best JL, Orfeo O, Vardy ME, Zinger JA. 2013. Decimeter-scale in situ mapping of modern cross-bedded dune deposits using parametric echo sounding: A new method for linking river processes and their deposits. *Geophysical Research Letters* 40(15): 3883-3887.

Sandbach SD, Nicholas AP, Ashworth PJ, Best JL, Keevil CE, Parsons DR, Prokocki EW, Simpson CJ. 2018. Hydrodynamic modelling of tidal-fluvial flows in a large river estuary. *Estuarine, Coastal and Shelf Science* 212: 176-188.

Scheidegger KF, Phipps JB. 1976. Dispersal patterns of sands in Grays Harbor Estuary, Washington. *Journal of Sedimentary Petrology* 46(1): 163-166.

Schippa L, Galvani I, Crose L, Pavan S. 2016. Multibeam surveying of river bed form and bed-load estimation at medium flow condition in a large sand river: Preliminary results of a field study in Po River. In River Flow 2016, Constantinescu G, Garcia M, Hanes D. (eds.), 1543-1550.

Sekiguchi T, Yokokawa M. 2008. Effect of wave period on combined-flow bedforms: a flume experiment. In Marine and River Dune Dynamics III, Parsons P, Garlan T, Best JL. (eds.). International Workshop, Leeds, U.K., 281-284.

Simenstad CA, Burke JL, O'Connor JE, Cannon C, Heatwolse DW, Ramiez MF, Waite IR, Counihan TD, Jones KL. 2011. Columbia River estuary ecosystem classification — concept and application. U.S. Geological Survey, *Open-File Report 2011-1228*, Reston.

Sherwood CR, Creager JS. 1990. Sedimentary geology of the Columbia River Estuary. *Progress in Oceanography* 25: 15-79.

Sherwood CR, Jay DA, Harvey RB, Hamilton P, Simenstad CA. 1990. Historical changes in the Columbia River Estuary. *Progress in Oceanography* 25: 299-352.

Smith JD, McLean SR. 1977. Spatially averaged flow over a wavy surface. *Journal of Geophysical Research* 82: 1735-1746.

Southard JB. 1991. Experimental determination of bed-form stability. *Annual Review of Earth and Planetary Sciences* 19: 423-455.

Southard JB, Boguchwal LA. 1990a. Bed configurations in steady unidirectional water flow part 1. Scale model study using fine sands. *Journal of Sedimentary Research* 60: 649-657.

Southard JB, Boguchwal LA. 1990b. Bed configurations in steady unidirectional water flow part 2. Synthesis of flume data. *Journal of Sedimentary Research* 60: 658-679.

Stolz A, Martin C, Wong C. 2005. Vertical control in a tidally influenced complex river system with a fixed low water datum. *Hydrographic Society of America Meeting,* 20-31.

Sukhodolov AN, Fedele JJ, Rhoads BL. 2006. Structure of flow over alluvial bed forms: an experiment on linking field and laboratory methods. *Earth Surface Processes and Landforms* 31: 1292-1310.

Sweet ML, Kocurek G. 1990. An empirical model of aeolian dune lee-face airflow. *Sedimentology* 37: 1023-1038.

Tanner WF. 1967. Ripple mark indices and their uses. *Sedimentology* 9(2): 89-104.

Templeton WJ, Jay DA. 2013. Lower Columbia River sand supply and removal: estimates of two sand budget components. *Journal of Waterway, Port, Coastal, and Ocean Engineering* 139(5): 383-392.

Unsworth CA, Nicholas AP, Ashworth PJ, Best JL, Lane SN, Parsons DR, Sambrook Smith GH, Simpson CJ, Strick RJP. 2020. Influence of dunes on channel-scale flow and sediment transport in a sand bed braided river. *Journal of Geophysical Research: Earth Surface* 125: *e2020JF005571*. doi:10.1029/2020JF005571.

van de Lageweg WI, Feldman H. 2018. Process-based modelling of morphodynamics and bar architecture in confined basins with fluvial and tidal currents. *Marine Geology* 398: 35-47.

van de Lageweg WI, Braat L, Parsons DR, Kleinhans MG. 2018. Controls on mud distribution and architecture along the fluvial-to-marine transition. *Geology* 46: 971-974.

Van den Berg JH, Boersma JR, Van Gelder A. 2007. Diagonostic sedimentary structures of the fluvial-tidal transition zone: evidence from deposits of the Rhine Delta. *Netherlands Journal of Geosciences/Geologie en Mijnbouw* 86(3): 287-306.

Van der Mark CF, Blom A, Hulscher SJMH. 2008. Quantification of variability in bedform geometry. *Journal of Geophysical Research* 113: F03020. doi:10.1029/2007JF000940.

Venditti JG. 2013. Bedforms in sand-bedded rivers. In Treatise on Geomorphology, Fluvial Geomorphology 9, Shroder JF, Wohl E. (eds.). *Academic Press, San Diego, CA,* 137-162.

Venditti JG, Bauer BO. 2005. Turbulent flow over a dune: Green River, Colorado. *Earth Surface Processes and Landforms* 30: 289-304. doi:10.1002/esp.1142.

Venditti JG, Church MA, Bennett SJ. 2005a. On the transition between 2D and 3D dunes. *Sedimentology* 526: 1343-1360.

Venditti JG, Church MA, Bennett SJ. 2005b. Bedform initiation from a flat sand bed. *Journal of Geophysical Research - Earth Surface* 110(F1): doi:10.1029/2004JF000149.

Viparelli E, Solari L, Hill KM. 2015. Downstream lightening and upward heavying: experiments with sediments differing in density. *Sedimentology* 62: 1384-1407.

Walton TL Jr., Adams WD. 1976. Capacity of inlet outer bars to store sand. *Proceedings American Society of Civil Engineers Part II: Coastal Sediment Problems*, 1919-1937.

Whetten JT, Kelley JC, Hanson LG. 1969. Characteristics of Columbia River sediment and sediment transport. *Journal of Sedimentary Petrology* 39(3): 1149-1166.

Williams JJ, Bell PS, Thorne PD. 2003. Field measurements of flow fields and sediment transport above mobile bed forms. *Journal of Geophysical Research* 108(C4): *3109*. doi:10.1029/2002JC001336.

Wright LD, Coleman JM, Thom BG. 1973. Processes of channel development in a high-tide-range environment: Cambridge Gulf-Ord River delta, Western Australia. *The Journal of Geology* 81: 15-41.

Wu S, Cheng H, Xu YJ, Li J, Zheng S, Xu W. 2016. Riverbed micromorphology of the Yangtze River Estuary, China. *Water* 8(5): 190. doi:10.3390/w8050190.

Yalin MS. 1964. Geometrical properties of sand waves. *Journal of Hydraulic Engineering* 90(5): 105-119.

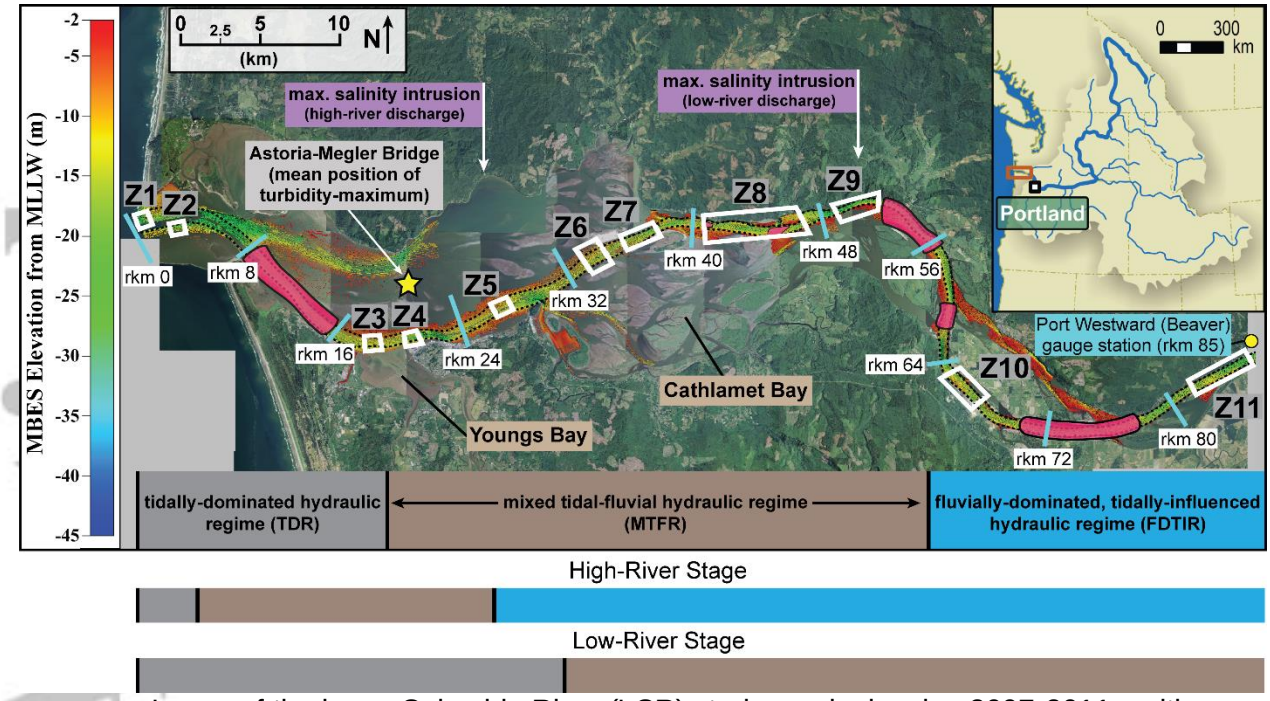

FIGURE 1 Image of the lower Columbia River (LCR) study reach showing 2007-2011 multi-beam echo sounding (MBES) data coverage of its main channel (dashed black line) provided by the National Oceanographic and Atmospheric Agency (NOAA). Included are: (a) the eleven zones where dune metrics were measured (z1-z11; open white rectangles), (b) the mean longitudinal extent of the three major fluvial-tidal hydraulic regimes as defined by Jay et al. (1990), as well as their inferred boundaries during high- and low- river stages (below the figure), (c) the upstream limits of salinity intrusion during high-and low- fluvial flows as reported by Fox et al. (1984) and Chawla et al. (2008), and (d) channel reaches most impacted by dredging of the federal navigation channel between 2005-2010 (pink rectangles). Elevations represent those from the Mean Lower Low Water (MLLW) level at the NOAA Astoria, OR, tide station (ID: 9439040). Refer to Figures 5-8 for detailed images of zones 1-11. Aerial image from US National Agriculture Imagery Program (NAIP) at https://gdg.sc.egov.usda.gov/.

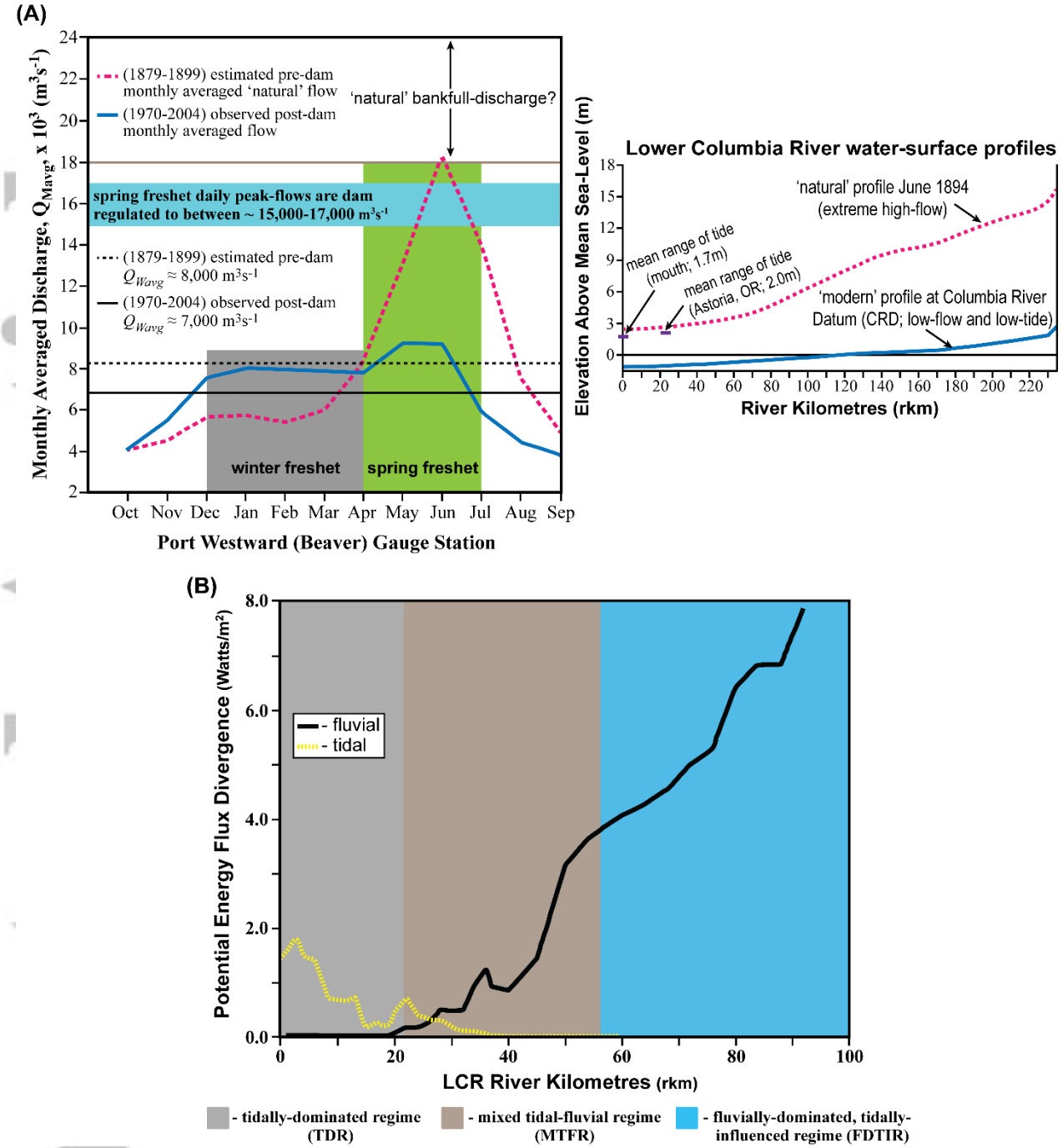

FIGURE 2 (A) Monthly averaged Lower Columbia River 'natural' (1879-1899; dashed pink line) *versus* irrigation-depleted and dam-regulated modern discharges (1970-2004; blue line) at the Port Westward (Beaver) gauge station. Also displayed are: i) 'natural' (dashed black line) *vs* post-dam (solid black line) mean annual discharges and ii) plot of low- and high- river stage water surface profiles. Modified from Naik and Jay (2011). (B) Graph displaying the time-averaged potential energy flux divergences of tidal (dashed yellow line) *vs* fluvial (black line) energy sources and mean boundaries of fluvial-tidal transition regimes as predicted by the model of Giese and Jay (1989) and Jay et al. (1990). Modified from Jay et al. (1990).

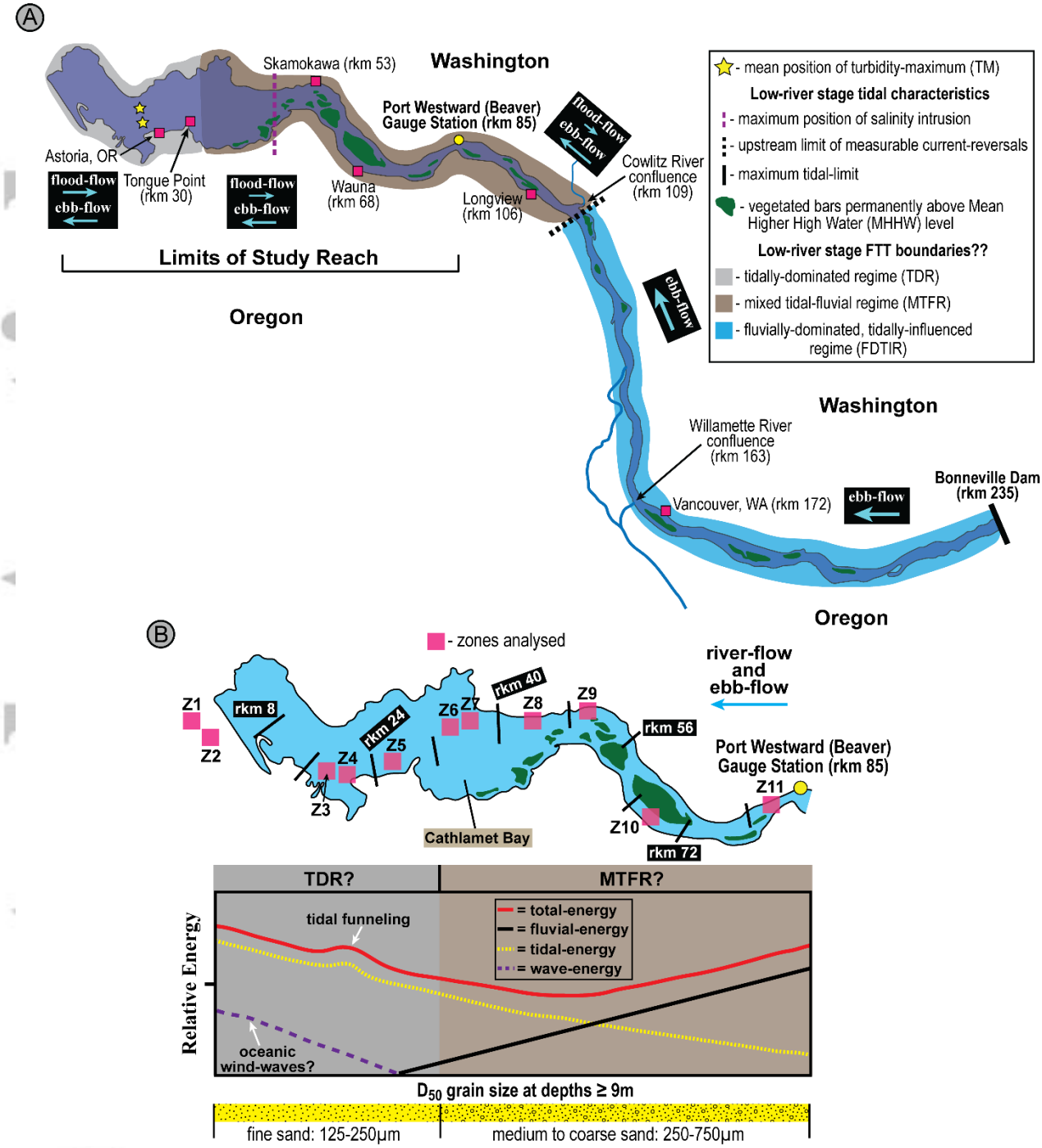

FIGURE 3 (A) Planform diagram of the Lower Columbia River (LCR) from rkm 0-235 displaying the inferred low-river stage boundaries of its fluvial-tidal transition hydraulic regimes as well as the limits and positions of relevant tidal characteristics. (B) Conceptual diagram illustrating the relative low-river stage hydrodynamic energy and modern channel bed D_{50} grain size at depths ≥ 9m.

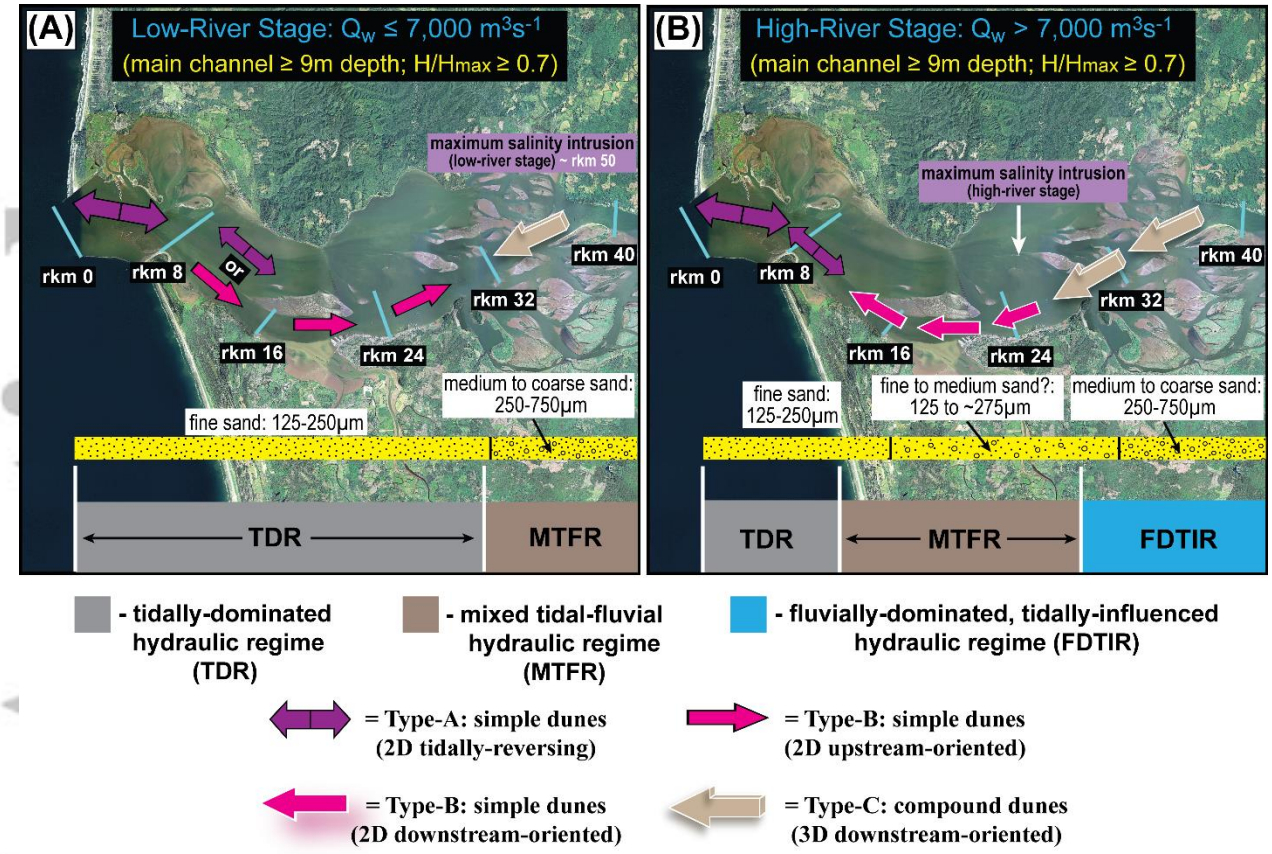

FIGURE 4 Distribution of primary dune morphology (≥ 9m depth; H/H_{max} ≥ 0.7) and channel bed grain size within the main channel of the Lower Columbia River from ~ rkm 0-35 as observed by Sherwood and Creager (1990). Data are from September 1979 to June 1980 over varying daily and spring-neap tidal-cycles during (A) low-river stages and (B) high-river stages. Note that fluvial-tidal transition regimes expand and contract as a function of river-stage. See Table 1 and main text for further descriptions of Type-A to C dunes. Adapted from Sherwood and Creager (1990).

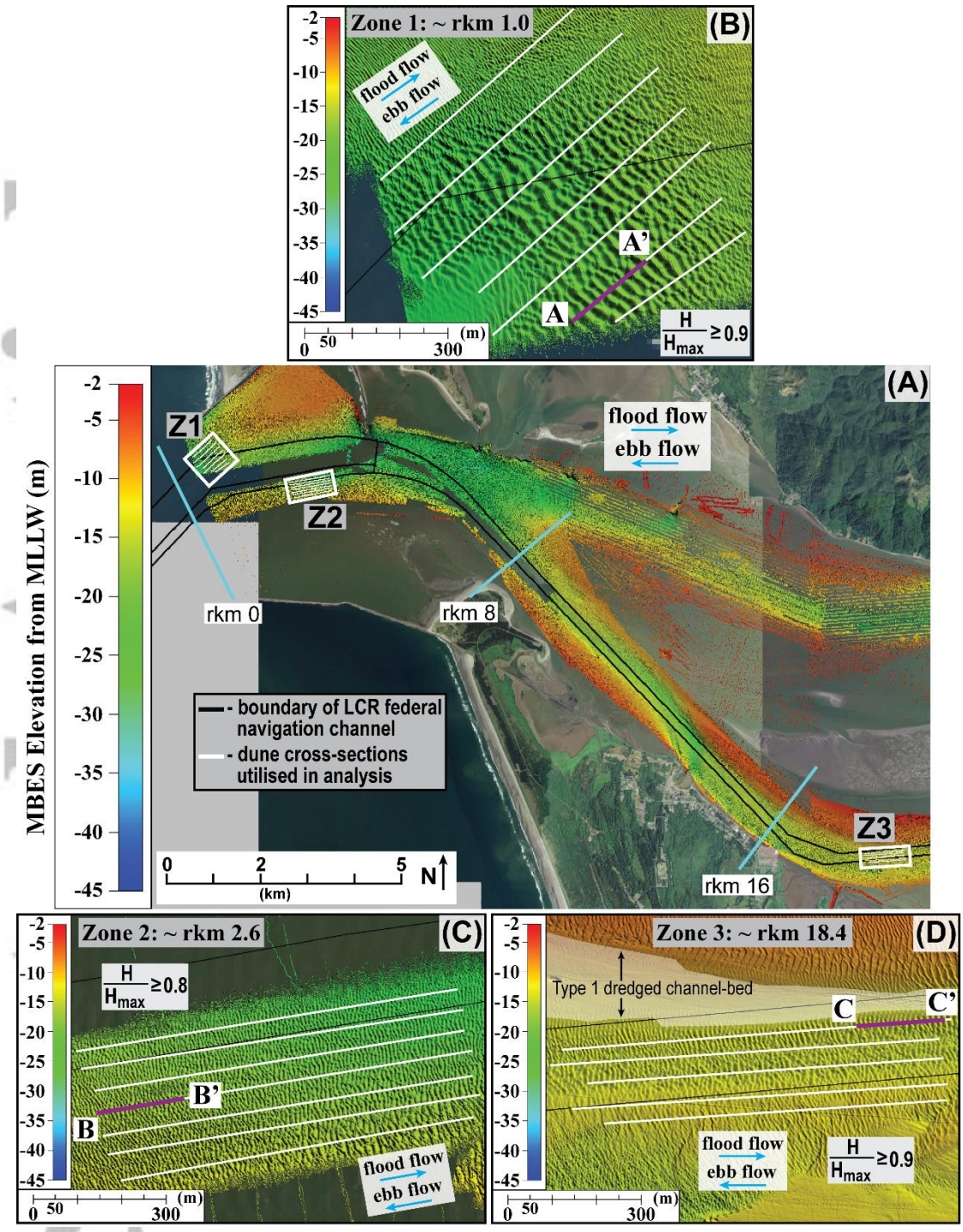

FIGURE 5 (A) Image of the lower Columbia River (LCR) displaying multi-beam echo sounding (MBES) data from ~ rkm 0-19 (zones 1-3; white rectangles) where primary bedforms were analysed with respect to the boundaries of the main navigation channel (black lines). (B-D) Magnified images of zones 1-3 showing the sections (white lines) utilised to quantify bedform metrics. Note that all bedforms examined are unmodified, because they lie outside of Type 1 or 2 dredged regions. See Figure 9 for partial sections A-A' to C-C' (purple lines).

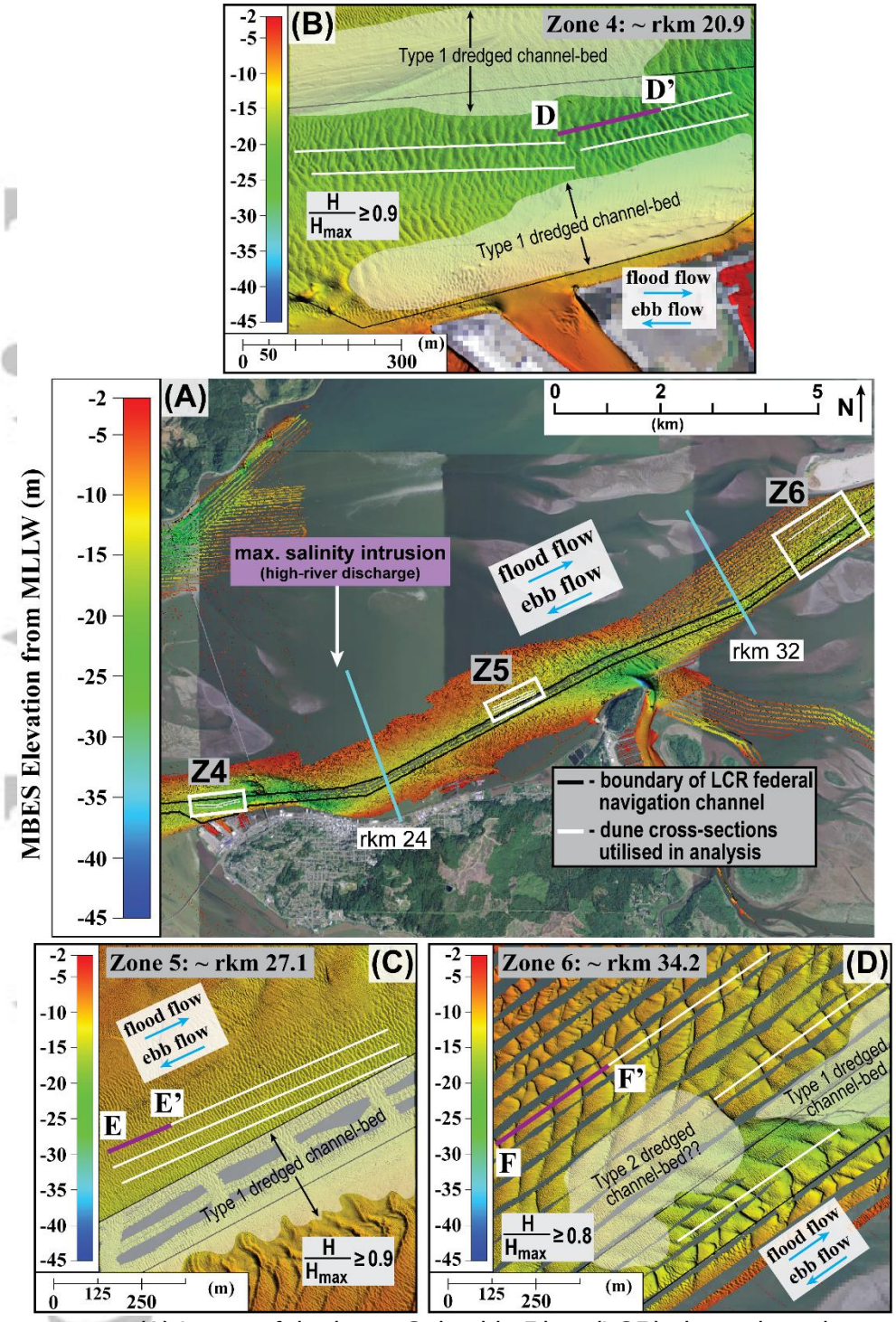

FIGURE 6 (A) Image of the lower Columbia River (LCR) channel reach ranging from ~ rkm 20-35, which displays multi-beam echo sounding (MBES) data of zones 4-6 (white rectangles) where primary bedforms were evaluated. (B-D) Magnified images of zones 4-6 showing the sections (white lines) used to quantify bedform metrics. All bedforms examined are unmodified because they formed outside of Type 1 or 2 dredged regions. See Figure 9 for partial sections D-D' to F-F' (purple lines).

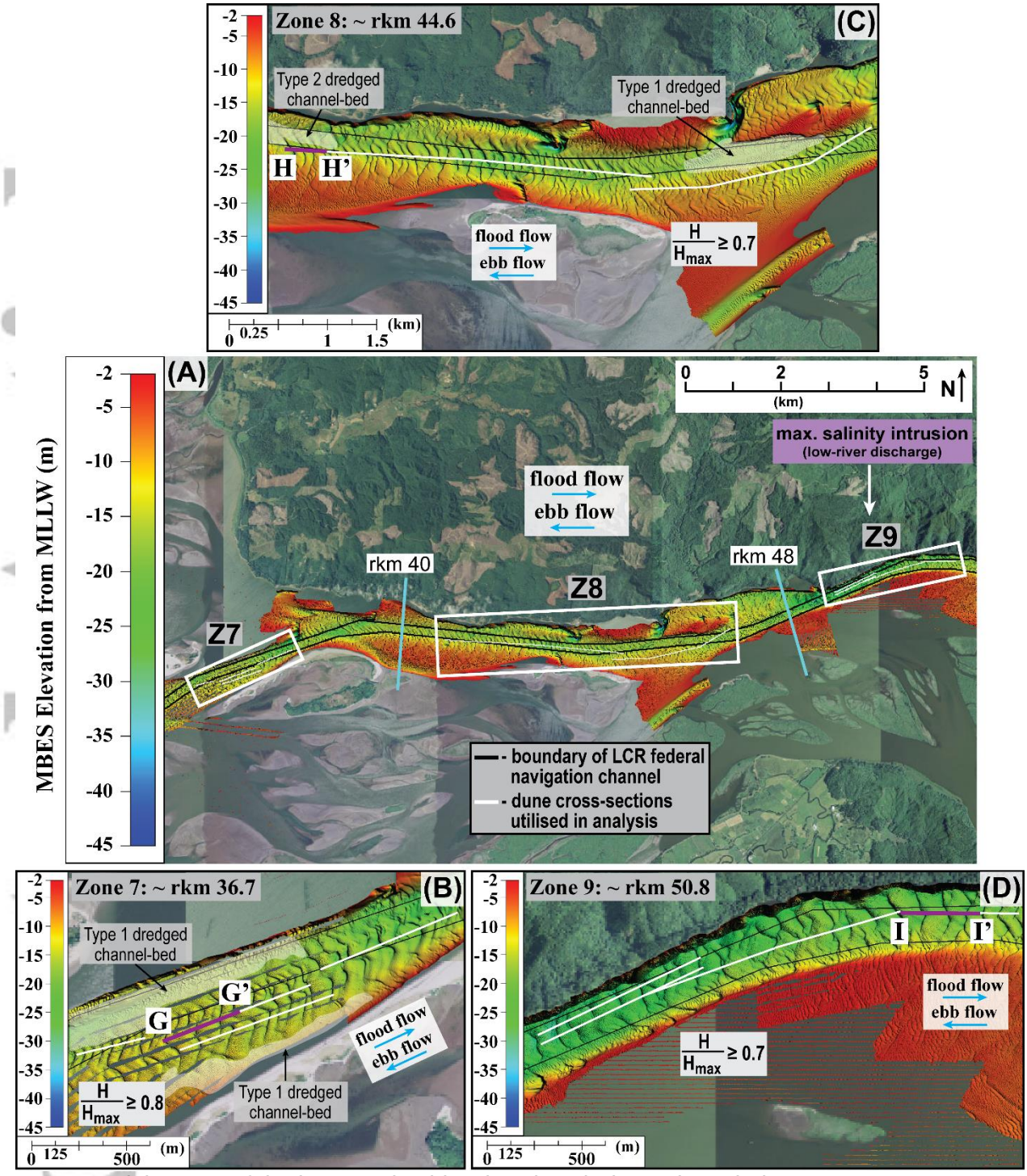

FIGURE 7 (A) Image of the lower Columbia River (LCR) channel reach that encompasses multi-beam echo sounding (MBES) data from ~ rkm 35-52 (zones 7-9; white rectangles) where primary bedforms were examined. (B-D) Magnified images of zones 7-9 displaying the sections (white lines) used to quantify bedform geometric properties. Note that all bedforms analysed exist outside of Type 1 and 2 dredged areas and are therefore unmodified. Refer to Figure 9 for partial sections G-G' to I-I' (purple lines).

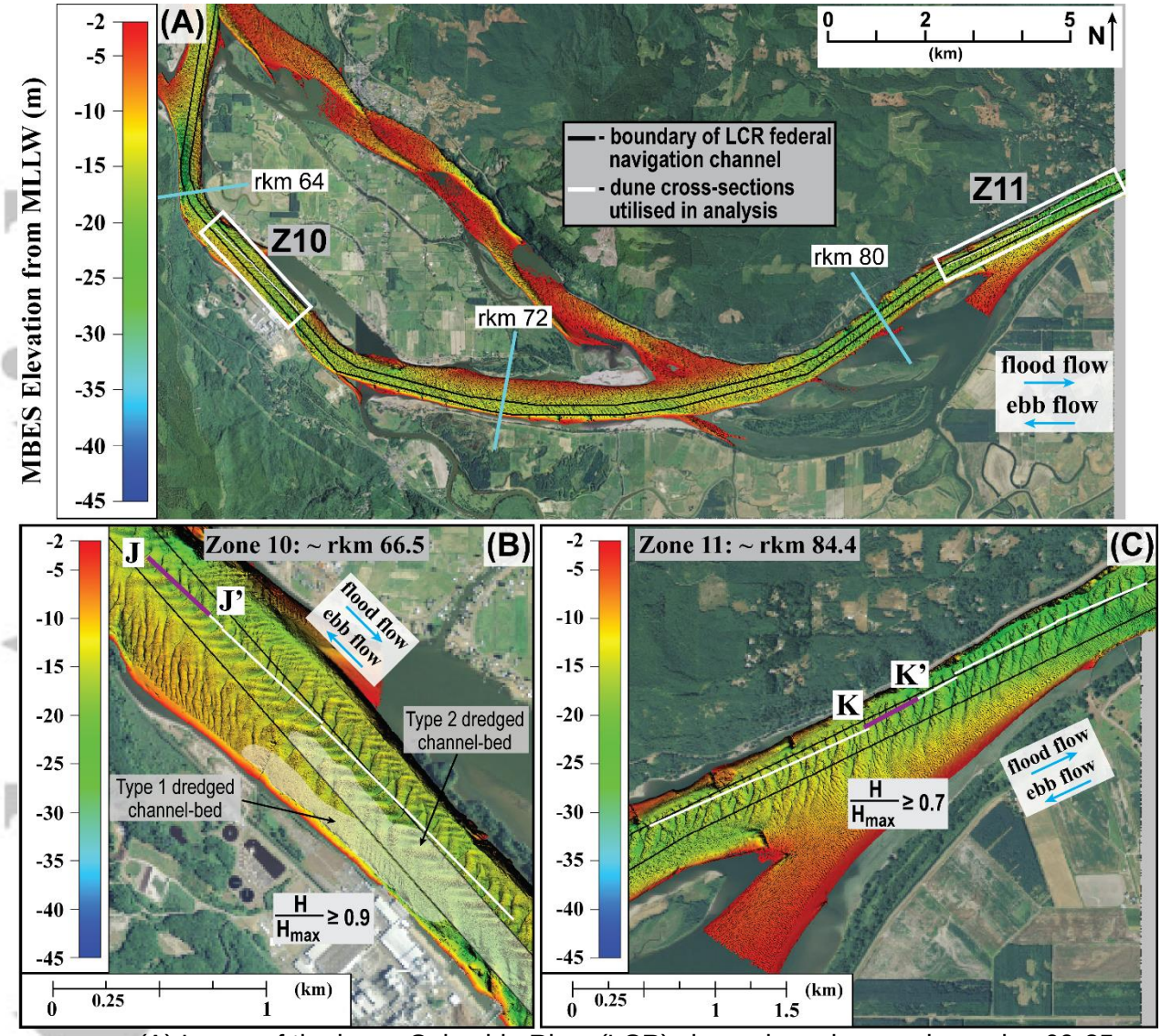

FIGURE 8 (A) Image of the lower Columbia River (LCR) channel reach spanning ~ rkm 60-85 that includes multibeam echo sounding (MBES) zones 10 and 11 (white rectangles) where primary bedforms were analysed. (B and C) Magnified images of zones 10 and 11 displaying the sections (white lines) used to quantify bedform metrics. Notice that all bedforms investigated are unmodified, because they occur outside of Type 1 or 2 dredged regions. See Figure 9 for partial sections J-J' to K-K' (purple lines).

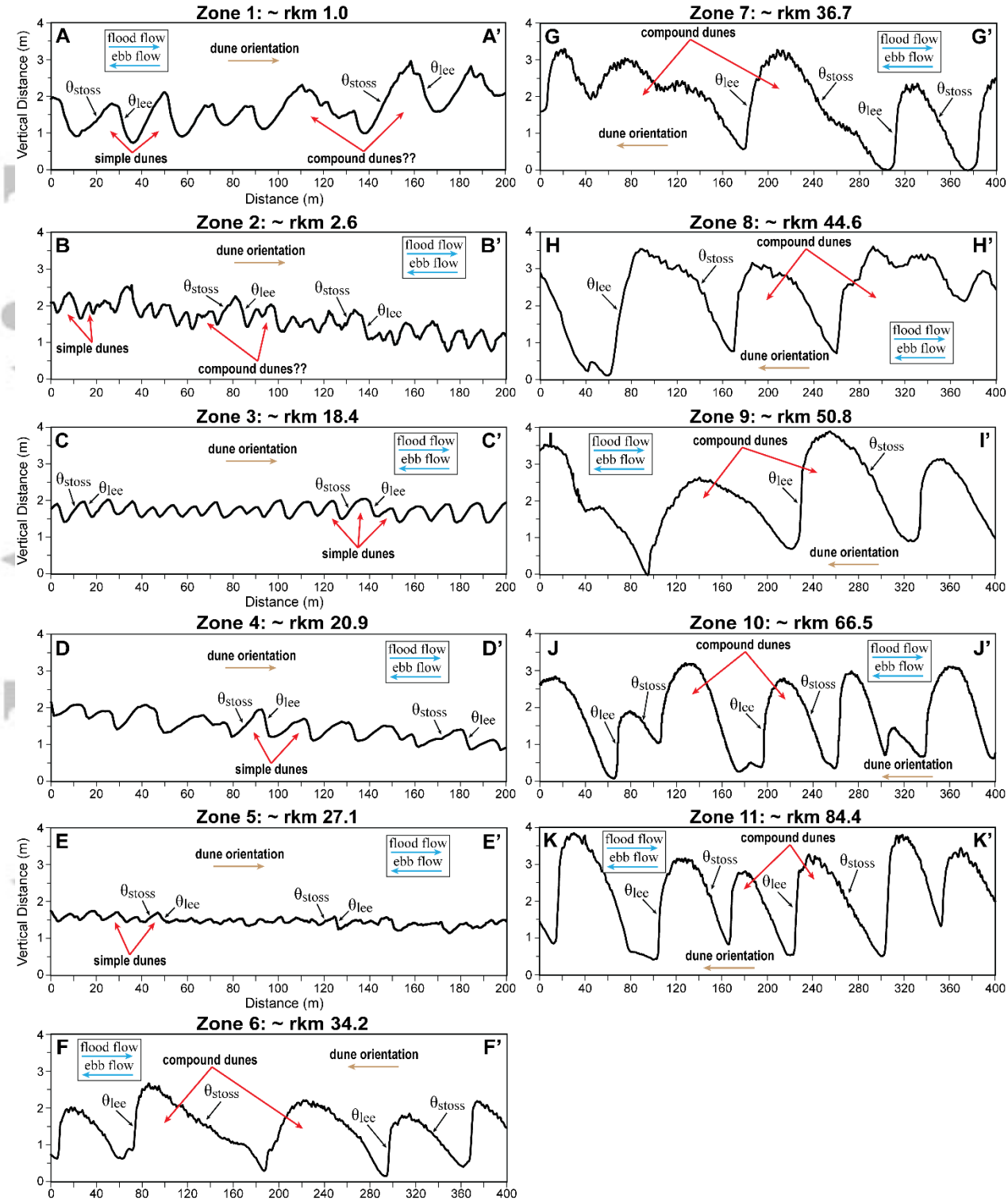

FIGURE 9 Examples of partial-sections A-A' to K-K' displaying bedform profiles of zones 1-11 (~ rkm 1.0-84.4) at low-river stage. The location of individual sections is shown in Figures 5-8 (purple lines).

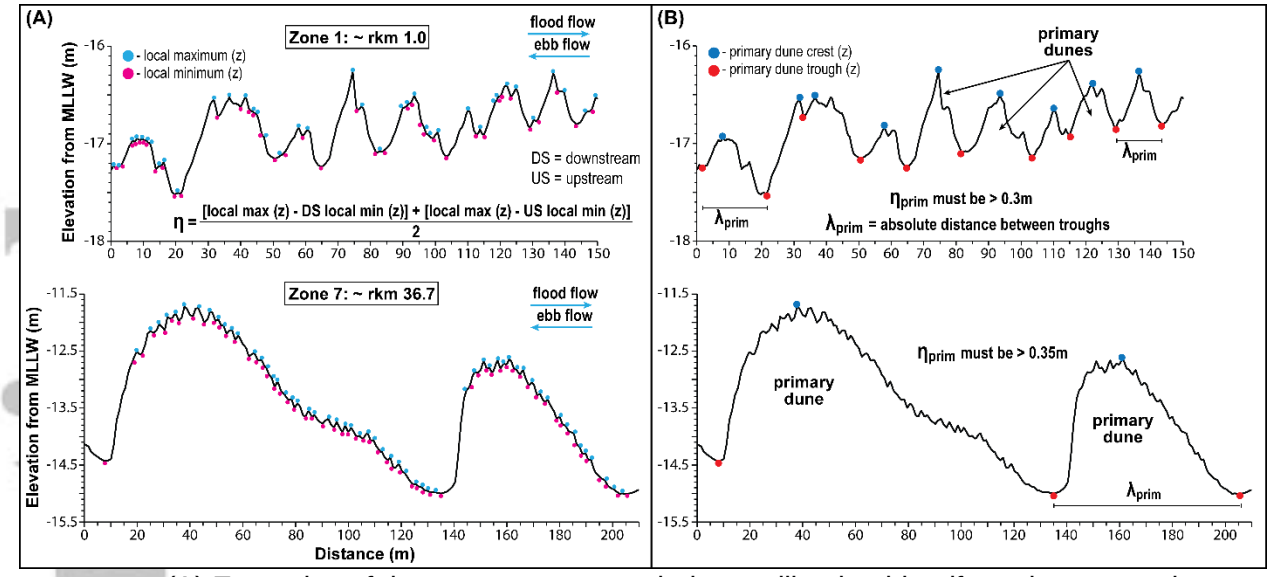

FIGURE 10 (A) Examples of the measurement technique utilised to identify and compute the heights (η) of all bedforms (both primary and secondary). (B) Identification and calculation procedures used to determine only primary dune wavelengths (λ_{prim}) after applying the primary dune height (η_{prim}) cut-offs associated with each zone example in (A). Note that η_{prim} must be greater than the largest η of secondary bedforms present in individual zones. See Table 3 for the primary dune height cut-offs applied to each zone.

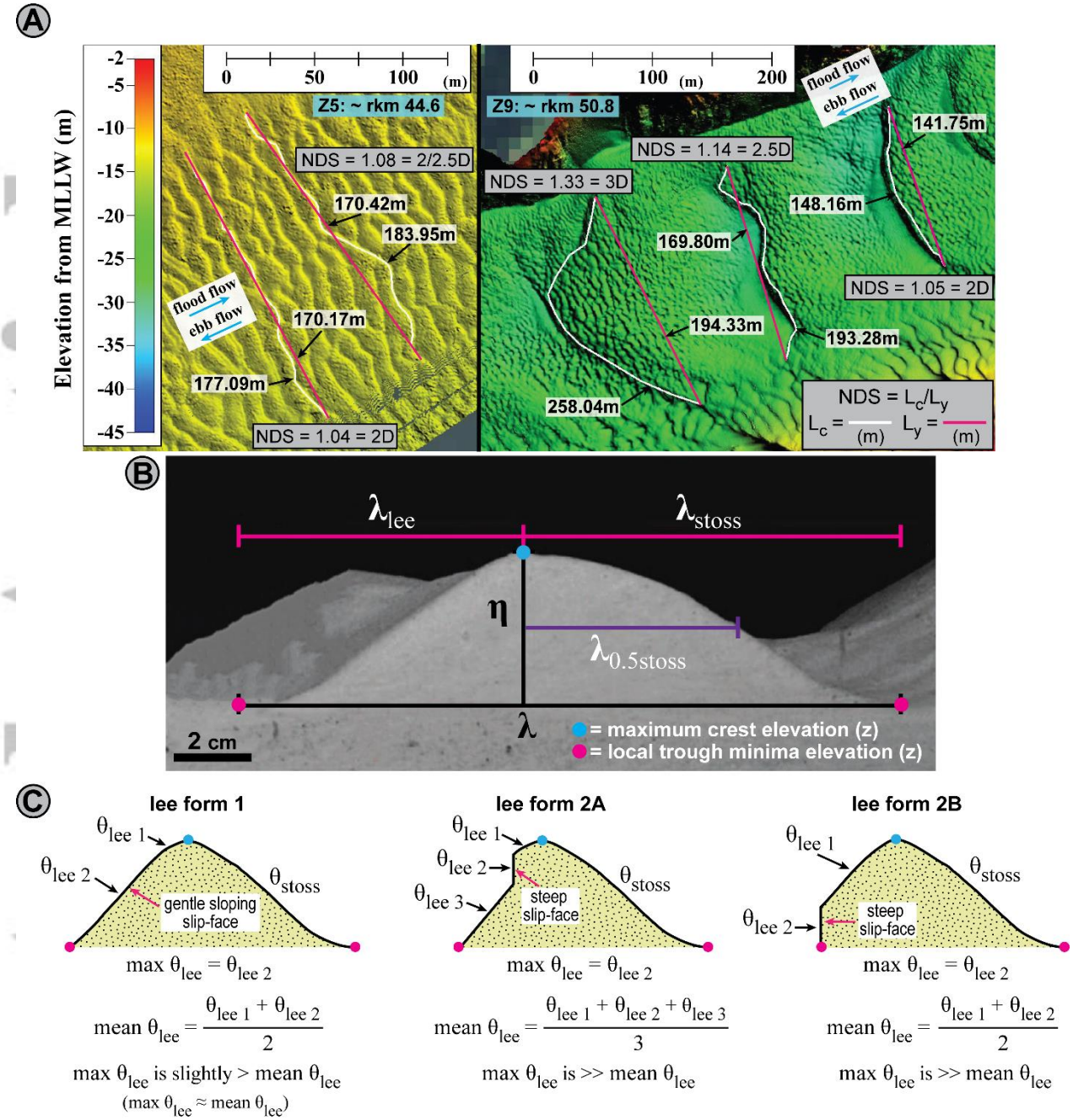

FIGURE 11 (A) Examples of the measurement technique used to calculate the non-dimensional span index, NDS, of primary dunes. See main text for dimensional regime boundaries. (B) Primary dune measurement parameters used in the calculations of bedform symmetry and roundness indices (BSI and BRI). Dune BSI and BRI values were obtained using Equations 3 and 4. Adapted from Perillo et al. (2014a). (C) Illustrations of the three forms of lee-side morphology present in the primary dunes of the lower Columbia River. Also shown are relationships used to compute maximum and mean lee-angles of various dune forms.

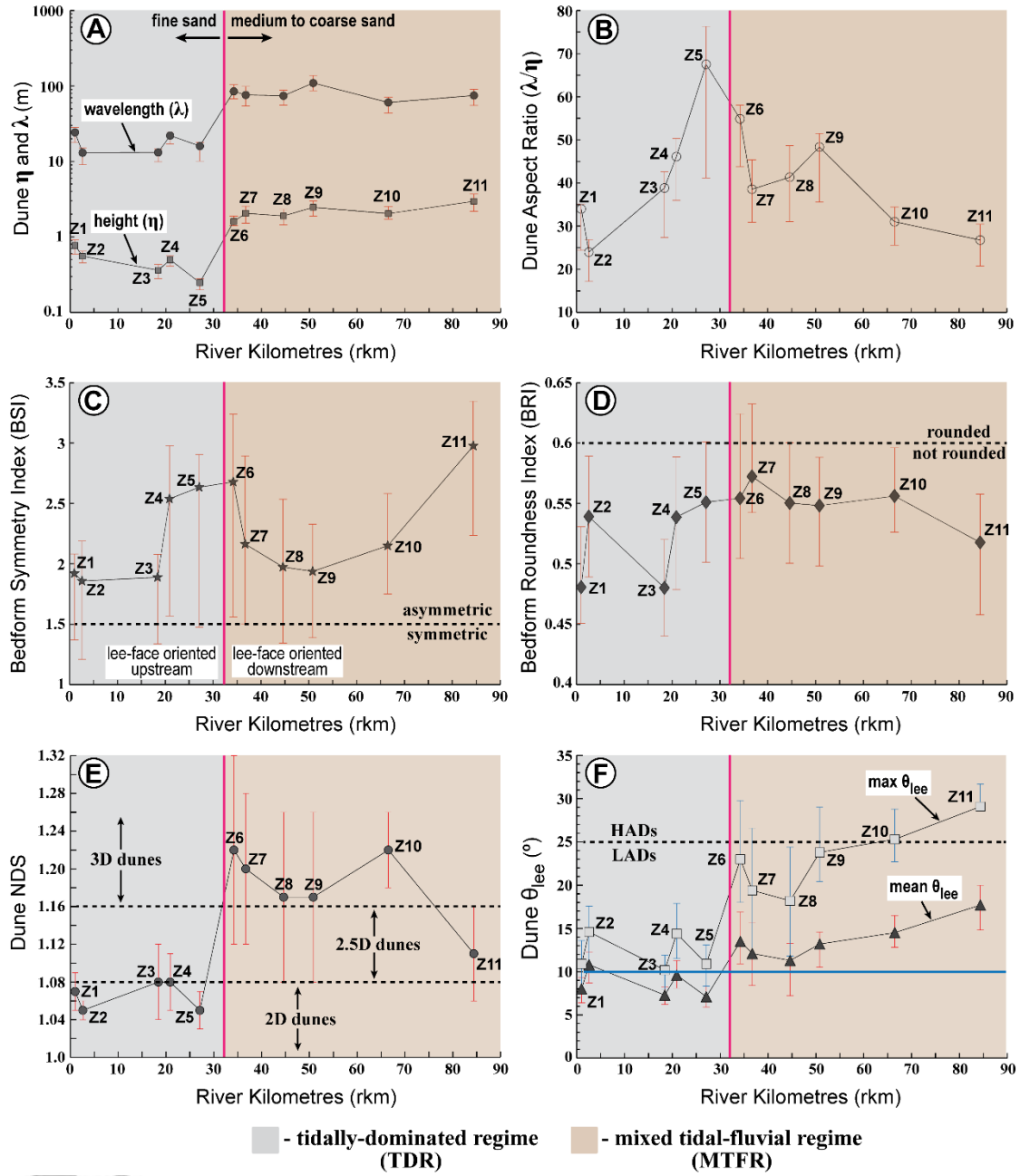

FIGURE 12 (A-F) Mean characteristics of primary dunes (≥ 9m depth; local H/H_{max} ≥ 0.7) throughout the fluvial-tidal transition of the lower Columbia River (LCR) at low-river stage. For (A-D) and (F), reported mean values are bracketed by error bars extending from the 25th to 75th quartiles of their gamma distributions, whilst in (E) error bars represent values at ± one σ from the arithmetic mean. The vertical pink solid line in (A-F) marks the transition between dunes composed of fine sand that are upstream oriented (below ~ rkm 32) and those composed of medium to coarse sand that are downstream oriented (above ~ rkm 32). The horizontal blue solid line in (F) denotes the mean θ_{lee} (~ 10°) of both deep (≥ 2.5m depth) rivers (Cisneros et al., 2020) and estuarine dunes (Dalrymple and Rhodes, 1995).

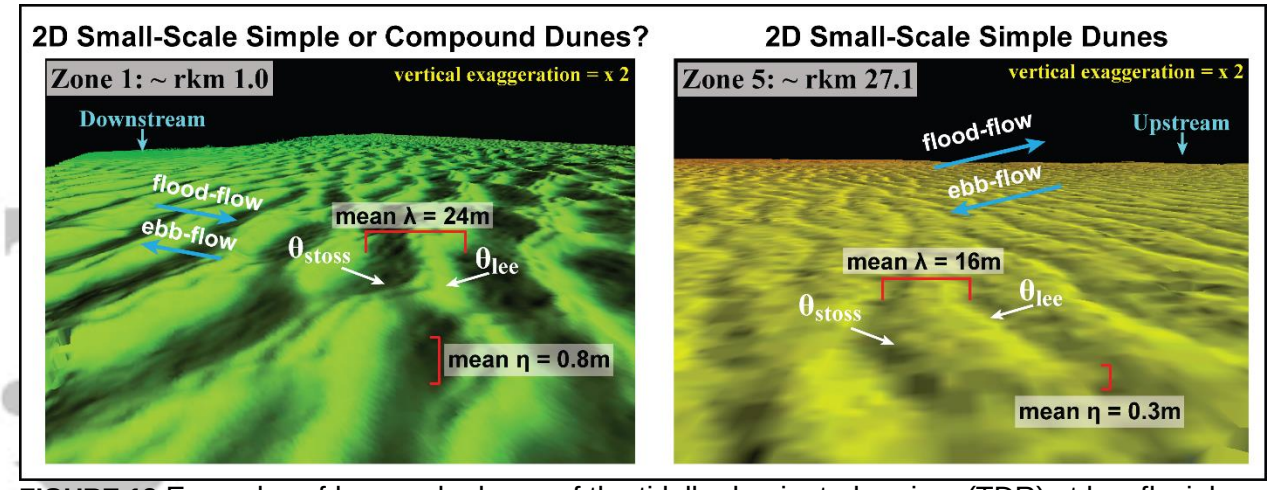

FIGURE 13 Examples of low-angle dunes of the tidally-dominated regime (TDR) at low-fluvial discharge (< 7,000 m^3s^{-1}).

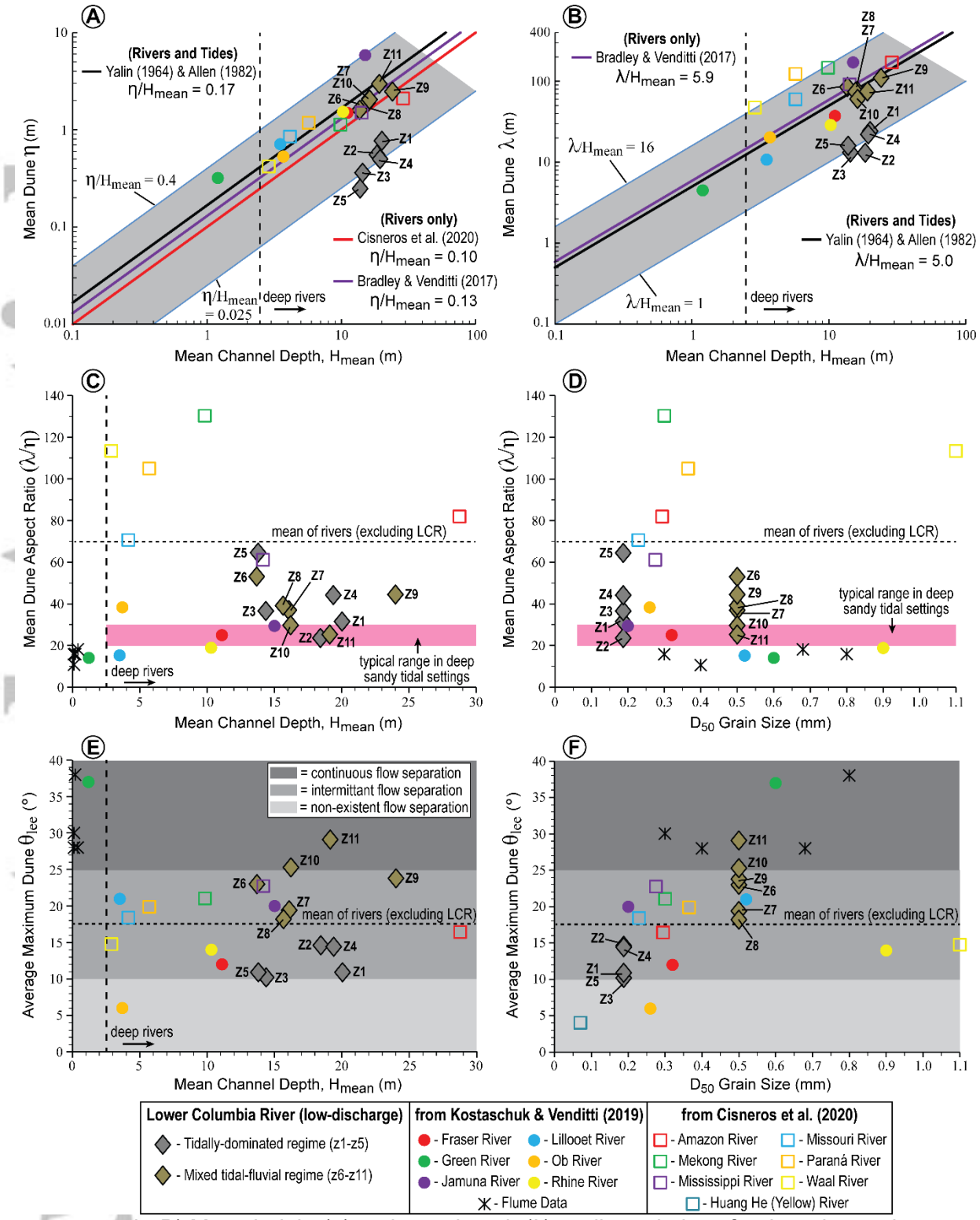

FIGURE 14 (A-B) Mean height (η) and wavelength (λ) scaling relations for the primary dunes (≥ 9m depth; local H/H_{max} ≥ 0.7) of the fluvial-tidal transition of the lower Columbia River as a function of mean channel depth (H_{mean}) relative to other fluvial (coloured circles and open squares) and estuarine environments (note that the grey shaded region bounds the scatter of data for both fluvial and tidal-estuarine settings). (C-D) Comparisons of the aspect ratio of dunes in the fluvial-tidal transition zone versus depth and grain size relative to those of other fluvial, flume, and estuarine settings. (E-F) Plots of maximum dune lee-angle in the fluvial-tidal transition zone versus those of other rivers and unidirectional flume experiments as a function of channel depth and grain size.

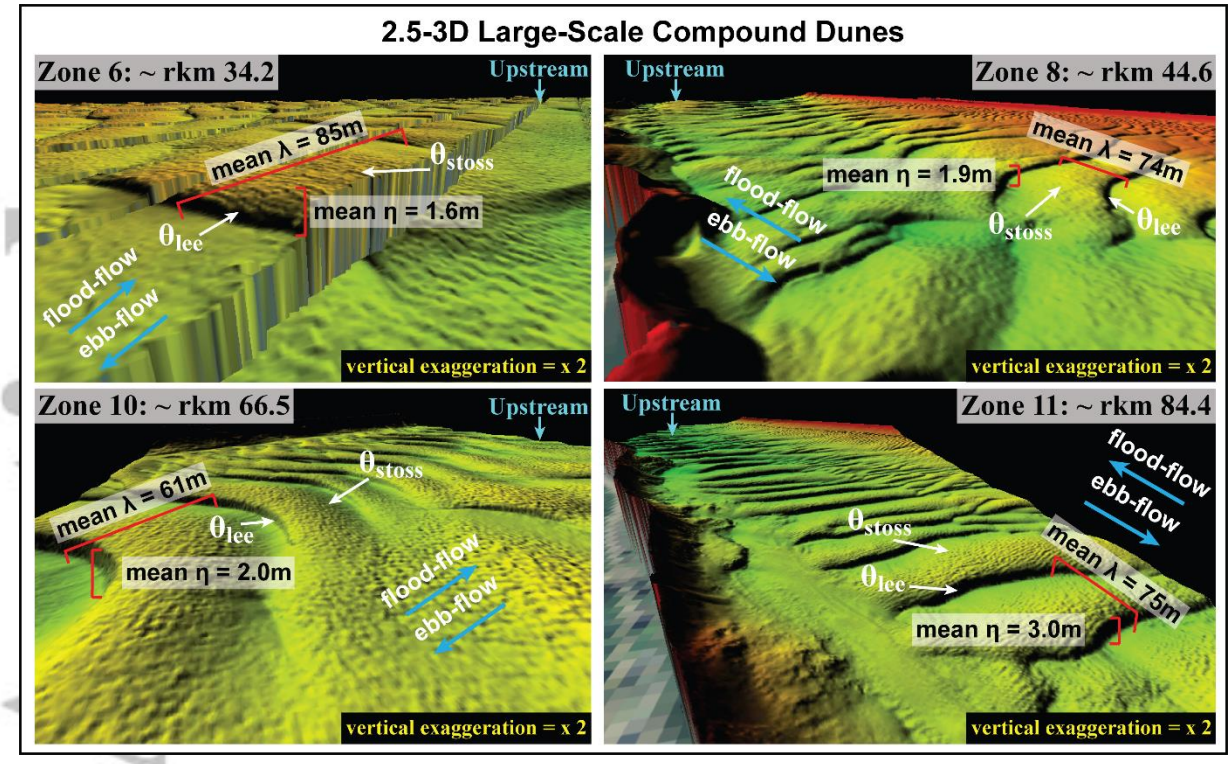

FIGURE 15 Examples of compound dunes within the mixed tidal-fluvial regime at low-fluvial discharge (< 7,000 m^3s^{-1}).

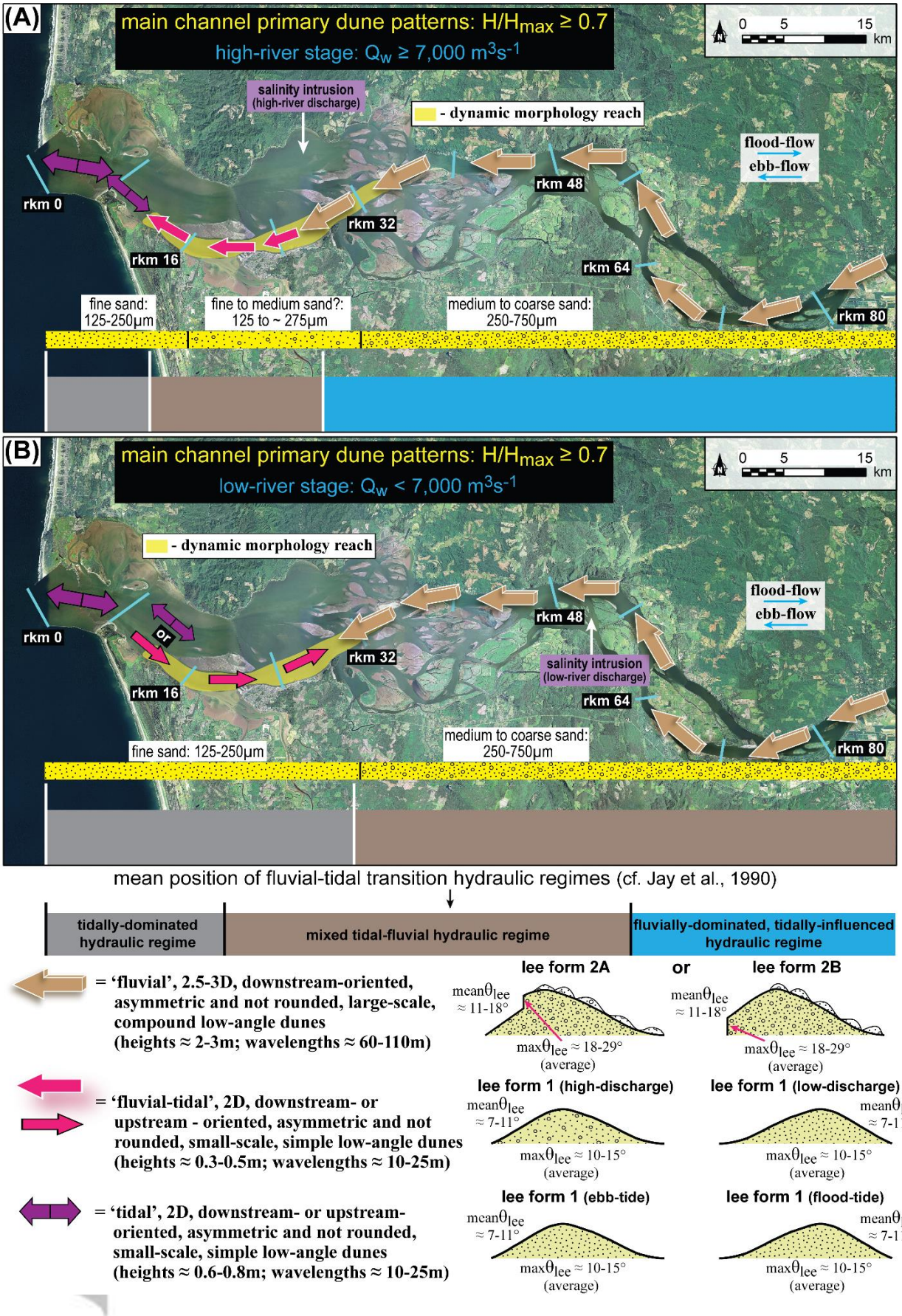

FIGURE 16 Comparison of morphology patterns and distributions of primary dunes in the fluvial-tidal transition (≥ 9m depth; local H/H_{max} ≥ 0.7) of the Lower Columbia River: (A)

high-river stage, and (B) low-river stage. ‘Fluvial’ dunes dominate throughout the fluvial-tidal transition (~86-90% of total), whilst ‘fluvial-tidal to tidal’ dunes are only present in the most seaward locations (~ 10-14% of total). Changes between high- and low- fluvial flows drives the expansion and contraction of the fluvial-tidal transition, which leads to development of a ‘dynamic morphology reach’ (~ rkm 12-35; highlighted in yellow) that experiences the greatest spatio-temporal variation in primary dune morphology. Results represent an integration of findings from the present study and Sherwood and Creager (1990) presented in Figure 4A, B.

Type-A: ~ rkm 0-9 (tidally-reversing during all river-stages)	
Dune Metric	Descriptions
height (η)	~ 0.2-1m
wavelength (λ)	~ 3-10m
aspect ratio (λ/η)	~ 10-20
†symmetry	asymmetric to symmetric
†roundness	commonly not-rounded to sporadically rounded
†dimensionality	2D in planform
†dune type	simple
Type-B: ~ rkm 9-30 (low-discharge ≤ 7,000 m^3s^{-1}); ~ rkm 9-24 (high-discharge > 7,000 m^3s^{-1})	
Dune Metric	Descriptions
height (η)	~ 0.3-0.9m
wavelength (λ)	~ 3-40m
aspect ratio (λ/η)	~ 35
†symmetry	asymmetric upstream-oriented (low-flow); asymmetric and downstream-oriented (high-flow)
†roundness	typically not-rounded
†dimensionality	2D in planform
†dune type	simple
Type-C: ~ rkm 30-35 (low-discharge ≤ 7,000 m^3s^{-1}); ~ rkm 24-35 (high-discharge > 7,000 m^3s^{-1})	
Dune Metric	Descriptions
height (η)	~ 1-3m
wavelength (λ)	≥ 100m
aspect ratio (λ/η)	~ 50
†symmetry	asymmetric to symmetric, and always downstream-oriented
†roundness	not-rounded to rounded
†dimensionality	3D in planform
†dune type	compound

† = qualitative description provided by Sherwood and Creager (1990)

TABLE 1 The types and properties of primary dunes (≥ 9m depth; localised H/H_{max} ≥ 0.7) in the lower Columbia River (LCR) observed by Sherwood and Creager (1990). Observations were restricted to between ~ rkm 0-35 and represent a mixture of observations from both high- and low- river stages. See Figure 4A,B for spatial distribution of Type A-C dunes.

Lower Columbia River MBES Channel Reach	Survey Time Interval	Average Fluvial-Discharge Q_{avg} (m^3s^{-1})	Prior Spring Freshet Peak Fluvial-Discharge Q_{wpeak} (m^3s^{-1})
~ Rkm 0-32 *Z1: ~ 1.0 *Z2: ~ 2.6 †Z3: ~ 18.4 †Z4: ~ 20.9 †Z5: ~ 27.1	Aug. 8th - Oct. 2nd, 2007	~ 3,600	May 5th, 2007: ~ 12,900
~ Rkm 32-40 ‡Z6: ~ 34.2 ‡Z7: ~ 36.7	Sept. 15th - Sept. 23rd, 2008	~ 4,100	June 6th, 2008: ~ 16,400
~ Rkm 48-96 ΩZ9: ~ 50.8 ΩZ10: ~ 66.5 ΩZ11: ~ 84.4	Oct. 8th, 2008 - Mar. 5th, 2009	~ 5,300	June 6th, 2008: ~ 16,400
~ Rkm 40-48 ΦZ8: ~ 44.6	Oct. 7th, 2010 - Jan. 23rd, 2011	~ 6,600	June 13th, 2010: ~ 16,800

***** = soundings collected using MBES systems including the Wärtsilä Seabeam/Elac 1180, Klien 5000, and Reson SeaBat 8125 and 8101, deployed amongst multiple vessels

† = soundings collected using MBES systems including the Wärtsilä Seabeam/Elac 1180, and Reson SeaBat 8125 and 8101, deployed between multiple vessels

‡ = soundings collected using MBES systems including the Wärtsilä Seabeam/Elac 1180, and Reson SeaBat 7125, tilted 8125, and 8101, deployed amongst multiple vessels

Ω = soundings collected using Reson SeaBat 7125 and 8101 MBES systems deployed between multiple vessels

Φ = soundings collected using a Kongsberg EM 2002 MBES system deployed on a singular vessel

TABLE 2 Time intervals and average flow-discharges during multi-beam echo sounding (MBES) surveys of the lower Columbia River main channel from ~ rkm 0-90 relative to the timing of prior spring freshet peak fluvial-discharge events. Note that prior peak discharges are ~ 2.5-4 times greater than the average discharges during the surveys. Included are the approximate river kilometre (rkm) positions of associated zone(s) where primary dune metrics were quantified. Note that: i) surveying periods for all zones occurred over differing neap-spring and flood-ebb tidal cycles, and ii) differences in vertical soundings between systems were corrected via normalisation to lead-line depth soundings in regions of data overlap. Values of Q_{avg} and Q_{wpeak} were acquired from the Port Westward (Beaver) USGS gauge station (ID: 14246900) positioned at ~ rkm 85.

LCR MBES Zone	Primary Dune Height Cut-Off (m)
Zone 1: ~ rkm 1.0	$\eta_{prim} > 0.3$
Zone 2: ~ rkm 2.6	$\eta_{prim} > 0.3$
Zone 3: ~ rkm 18.4	$\eta_{prim} > 0.15$
Zone 4: ~ rkm 20.9	$\eta_{prim} > 0.25$
Zone 5: ~ rkm 27.1	$\eta_{prim} > 0.15$
Zone 6: ~ rkm 34.2	$\eta_{prim} > 0.5$
Zone 7: ~ rkm 36.7	$\eta_{prim} > 0.35$
Zone 8: ~ rkm 44.6	$\eta_{prim} > 0.4$
Zone 9: ~ rkm 50.8	$\eta_{prim} > 0.4$
Zone 10: ~ rkm 66.5	$\eta_{prim} > 0.4$
Zone 11: ~ rkm 84.4	$\eta_{prim} > 0.5$

TABLE 3 Primary dune height cut-offs for the eleven zones analysed. Bedforms possessing heights below the reported cut-offs are considered secondary bedforms and were not included in the final geometric analysis of primary dunes.

Zone 1: rkm 1.0	Distribution	N	Range	Mean	STD	Median	General Morphology
height (η)	Gamma	113	~ 0.4-1.6m	0.8m	±0.3	0.7m	-
wavelength (λ)	Gamma	113	~ 10-65m	24.3m	±9.0	21.5m	-
aspect ratio (λ/η)	Gamma	113	~ 20-160	34.0	±14.1	28.3	-
BSI	Gamma	113	~ 1-11	1.9	±0.8	1.7	asymmetric
BRI	Gamma	113	~ 0.2-0.7	0.5	±0.1	0.5	not rounded
mean θ_{lee}	Gamma	113	~ 4-16°	8.0°	±2.2	7.7°	LADs
max θ_{lee}	Gamma	113	~ 3-26°	10.9°	±4.4	10.3°	LADs
NDS	Arithmetic	10	1.05-1.11	1.07	±0.02	-	2D
dune form	-	-	-	-	-	-	simple to compound
H_{mean}	-	-	-	20.0m	-	-	-
η_{mean}/H_{mean}	-	-	-	0.04	-	-	-
λ_{mean}/H_{mean}	-	-	-	1.2	-	-	-
Zone 2: rkm 2.6	Distribution	N	Range	Mean	STD	Median	General Morphology
height (η)	Gamma	444	~ 0.3-1.3m	0.6m	±0.1	0.5m	-
wavelength (λ)	Gamma	444	~ 5-40m	13.1m	±5.4	11.2m	-
aspect ratio (λ/η)	Gamma	444	~ 10-95	24.0	±9.2	20.1	-
BSI	Gamma	444	~ 1-6	1.9	±0.8	1.5	asymmetric
BRI	Gamma	444	~ 0.2-0.9	0.5	±0.1	0.5	not rounded
mean θ_{lee}	Gamma	444	~ 6-20°	10.8°	±2.7	10.4°	LADs
max θ_{lee}	Gamma	444	~ 5-33°	14.6°	±5.5	13.8°	LADs
NDS	Arithmetic	12	1.02-1.05	1.05	±0.01	-	2D
dune form	-	-	-	-	-	-	simple to compound
H_{mean}	-	-	-	18.4m	-	-	-
η_{mean}/H_{mean}	-	-	-	0.03	-	-	-
λ_{mean}/H_{mean}	-	-	-	0.7	-	-	-
Zone 3: rkm 18.4	Distribution	N	Range	Mean	STD	Median	General Morphology
height (η)	Gamma	309	~ 0.2-0.7m	0.4m	±0.1	0.4m	-
wavelength (λ)	Gamma	309	~ 2-50m	13.2m	±4.8	11.7m	-
aspect ratio (λ/η)	Gamma	309	~ 20-160	39.0	±16.1	32.0	-
BSI	Gamma	309	~ 1-8	1.9	±0.7	1.7	asymmetric
BRI	Gamma	309	~ 0.2-0.8	0.5	±0.1	0.5	not rounded
mean θ_{lee}	Gamma	309	~ 5-13°	7.3°	±1.5	7.2°	LADs
max θ_{lee}	Gamma	309	~ 4-21°	10.2°	±3.1	9.9°	LADs
NDS	Arithmetic	44	1.02-1.21	1.08	±0.04	-	2/2.5D
dune form	-	-	-	-	-	-	simple
H_{mean}	-	-	-	14.4m	-	-	-
η_{mean}/H_{mean}	-	-	-	0.03	-	-	-
λ_{mean}/H_{mean}	-	-	-	0.9	-	-	-

Table 4 continued.

Zone 4: rkm 20.9	Distribution	N	Range	Mean	STD	Median	General Morphology
height (η)	Gamma	70	~ 0.3-0.8m	0.5m	±0.1	0.5m	-
wavelength (λ)	Gamma	70	~ 10-50m	22.0m	±7.1	21.2m	-
aspect ratio (λ/η)	Gamma	70	~ 30-150	46.1	±15.8	40.9	-
BSI	Gamma	70	~ 1-10	2.5	±1.3	2.1	asymmetric
BRI	Gamma	70	~ 0.3-0.8	0.5	±0.1	0.5	not rounded
mean θ_{lee}	Gamma	70	~ 5-15°	9.6°	±2.4	9.2°	LADs
max θ_{lee}	Gamma	70	~ 6-25°	14.4°	±4.8	13.6°	LADs
NDS	Arithmetic	12	1.05-1.15	1.08	±0.03	-	2/2.5D
dune form	-	-	-	-	-	-	simple
H_{mean}	-	-	-	19.4m	-	-	-
η_{mean}/H_{mean}	-	-	-	0.03	-	-	-
λ_{mean}/H_{mean}	-	-	-	1.1	-	-	-
Zone 5: rkm 27.1	Distribution	N	Range	Mean	STD	Median	General Morphology
height (η)	Gamma	222	~ 0.2-0.5m	0.3m	±0.1	0.2m	-
wavelength (λ)	Gamma	222	~ 10-110m	16.0m	±7.9	12.1m	-
aspect ratio (λ/η)	Gamma	222	~ 50-450	67.5	±37.6	50.5	-
BSI	Gamma	222	~ 2-22	2.6	±1.5	2.1	asymmetric
BRI	Gamma	222	~ 0.2-0.8	0.6	±0.1	0.6	not rounded
mean θ_{lee}	Gamma	222	~ 4-13°	7.1°	±1.9	6.8°	LADs
max θ_{lee}	Gamma	222	~ 4-22°	10.9°	±3.7	10.2°	LADs
NDS	Arithmetic	12	1.03-1.09	1.05	±0.02	-	2D
dune form	-	-	-	-	-	-	simple
H_{mean}	-	-	-	13.8m	-	-	-
η_{mean}/H_{mean}	-	-	-	0.02	-	-	-
λ_{mean}/H_{mean}	-	-	-	1.2	-	-	-
Zone 6: rkm 34.2	Distribution	N	Range	Mean	STD	Median	General Morphology
height (η)	Gamma	22	~ 0.6-2.1m	1.6m	±0.4	1.6m	-
wavelength (λ)	Gamma	22	~ 45-125m	85.0m	±23.7	82.4m	-
aspect ratio (λ/η)	Gamma	22	~ 35-95	54.9	±15.4	52.8	-
BSI	Gamma	22	~ 1-7	2.7	±1.4	2.0	asymmetric
BRI	Gamma	22	~ 0.3-0.7	0.6	±0.10	0.6	not rounded
mean θ_{lee}	Gamma	22	~ 7-20°	13.5°	±3.9	13.9°	LADs
max θ_{lee}	Gamma	22	~ 10-36°	23.0°	±7.7	23.9°	LADs
NDS	Arithmetic	6	1.10-1.33	1.22	±0.1	-	3D
dune form	-	-	-	-	-	-	compound
H_{mean}	-	-	-	13.7m	-	-	-
η_{mean}/H_{mean}	-	-	-	0.12	-	-	-
λ_{mean}/H_{mean}	-	-	-	6.2	-	-	-

Table 4 continued.

Zone 7: rkm 36.7	Distribution	N	Range	Mean	STD	Median	General Morphology
height (η)	Gamma	44	~ 0.5-4m	2.0m	±0.8	2.1m	-
wavelength (λ)	Gamma	44	~ 20-130m	76.0m	±30.7	72.0m	-

aspect ratio (λ/η)	Gamma	44	~ 20-85	38.6	±12.0	37.4	-
BSI	Gamma	44	~ 1-4.3	2.2	±0.8	2.0	asymmetric
BRI	Gamma	44	~ 0.4-0.8	0.6	±0.1	0.6	not rounded
mean θ_{lee}	Gamma	44	~ 4-19°	12.1°	±4.3	12.6°	LADs
max θ_{lee}	Gamma	44	~ 4-32°	19.4°	±8.6	20.4°	LADs
NDS	Arithmetic	14	1.07-1.33	1.20	±0.08	-	3D
dune form	-	-	-	-	-	-	compound
H_{mean}	-	-	-	16.1m	-	-	-
η_{mean}/H_{mean}	-	-	-	0.13	-	-	-
λ_{mean}/H_{mean}	-	-	-	4.7	-	-	-

Zone 8: rkm 44.6	Distribution	N	Range	Mean	STD	Median	General Morphology
height (η)	Gamma	50	~ 1-4m	1.9m	±0.7	1.8m	-
wavelength (λ)	Gamma	50	~ 30-170m	74.3m	±25.4	73.3m	-
aspect ratio (λ/η)	Gamma	50	~ 25-85	41.4	±12.7	38.9	-
BSI	Gamma	50	~ 1.2-3.7	2.0	±0.7	1.8	asymmetric
BRI	Gamma	50	~ 0.3-0.7	0.6	±0.1	0.6	not rounded
mean θ_{lee}	Gamma	50	~ 4-17°	11.3°	±3.6	9.2°	LADs
max θ_{lee}	Gamma	50	~ 4-30°	18.2°	±7.2	18.8°	LADs
NDS	Arithmetic	19	1.07-1.51	1.17	±0.09	-	3D
dune type	-	-	-	-	-	-	Compound
H_{mean}	-	-	-	15.7m	-	-	-
η_{mean}/H_{mean}	-	-	-	0.12	-	-	-
λ_{mean}/H_{mean}	-	-	-	4.7	-	-	-

Zone 9: rkm 50.8	Distribution	N	Range	Mean	STD	Median	General Morphology
height (η)	Gamma	34	~ 0.8-4.5m	2.5m	±1.0	2.4m	-
wavelength (λ)	Gamma	34	~ 30-160m	109.7m	±40.0	114.7m	-
aspect ratio (λ/η)	Gamma	34	~ 30-120	48.3	±17.8	40.9	-
BSI	Gamma	34	~ 1-3.5	1.9	±0.6	1.9	asymmetric
BRI	Gamma	34	~ 0.4-0.7	0.6	±0.1	0.6	not rounded
mean θ_{lee}	Gamma	34	~ 7-21°	13.2°	±3.6	12.8°	LADs
max θ_{lee}	Gamma	34	~ 12-36°	23.8°	±6.3	23.2°	LADs
NDS	Arithmetic	16	1.05-1.33	1.17	±0.09	-	3D
dune type	-	-	-	-	-	-	compound
H_{mean}	-	-	-	24.0m	-	-	-
η_{mean}/H_{mean}	-	-	-	0.10	-	-	-
λ_{mean}/H_{mean}	-	-	-	4.6	-	-	-

Table 4 continued.

Zone 10: rkm 66.5	Distribution	N	Range	Mean	STD	Median	General Morphology
height (η)	Gamma	34	~ 0.8-3.3m	2.0m	±0.8	2.2m	-
wavelength (λ)	Gamma	34	~ 20-100m	60.5m	±21.5	57.4m	-
aspect ratio (λ/η)	Gamma	34	~ 20-50	31.0	±7.6	29.9	-
BSI	Gamma	34	~ 1-4.5	2.2	±0.7	2.1	asymmetric
BRI	Gamma	34	~ 0.3-0.7	0.6	±0.1	0.6	not rounded
mean θ_{lee}	Gamma	34	~ 6-20°	14.5°	±3.4	15.4°	LADs

max θ_{lee}	Gamma	34	~ 9-36°	25.3°	±6.3	26.2°	HADs
NDS	Arithmetic	13	1.18-1.28	1.22	±0.04	-	3D
dune type	-	-	-	-	-	-	compound
H_{mean}	-	-	-	16.2m	-	-	-
η_{mean}/H_{mean}	-	-	-	0.13	-	-	-
λ_{mean}/H_{mean}	-	-	-	3.7	-	-	-
Zone 11: rkm 84.4							
	Distribution	N	Range	Mean	STD	Median	General Morphology
height (η)	Gamma	46	~ 0.8-5m	3.0m	±1.1	2.9m	-
wavelength (λ)	Gamma	46	~ 30-140m	74.9m	±23.2	72.0m	-
aspect ratio (λ/η)	Gamma	46	~ 15-55	26.8	±7.8	24.9	-
BSI	Gamma	46	~ 1.5-6.5	3.0	±1.1	2.6	asymmetric
BRI	Gamma	46	~ 0.4-0.7	0.5	±0.1	0.5	not rounded
mean θ_{lee}	Gamma	46	~ 8-33°	17.7°	±5.2	17.1°	LADs
max θ_{lee}	Gamma	46	~ 13-34°	29.1°	±4.6	29.9°	HADs
NDS	Arithmetic	18	1.05-1.25	1.11	±0.05	-	2.5D
dune type	-	-	-	-	-	-	compound
H_{mean}	-	-	-	19.1m	-	-	-
η_{mean}/H_{mean}	-	-	-	0.15	-	-	-
λ_{mean}/H_{mean}	-	-	-	3.9	-	-	-

TABLE 4 Primary dune (≥ 9m depth; local H/H_{max} ≥ 0.7) characteristics throughout the fluvial-tidal transition of the lower Columbia River at low-river discharge. Standard deviations (STD) are at ± one σ from mean values. Note that zones within the tidally-dominated and mixed tidal-fluvial regimes are highlighted in grey and tan, respectively.